EES Catalysis

PERSPECTIVE

View Article Online
View Journal | View Issue

Cite this: *EES Catal.*, 2024, 2, 1072

Shining light on hybrid perovskites for photoelectrochemical solar to fuel conversion

Sudhanshu Shukla, *[abc] Vishal Jose[abc] and Nripan Mathews *[de]

Received 28th April 2024,
Accepted 16th July 2024

DOI: 10.1039/d4ey00091a

rsc.li/eescatalysis

Hybrid halide perovskites (HaPs) represent a class of material with excellent optoelectronic properties providing distinct avenues for disruptive photo(-electro) catalytic technologies. However, their photocatalytic activity, selectivity and stability remains a scientific and technological hurdle. In this perspective, we discuss fundamental aspects of perovskite based photocatalytic systems, specifically for CO_2 conversion and high value oxidation reactions, and highlight critical limiting factors and on-going challenges in the field. We critically assess the recent advances in designing halide perovskite hetero-interfaces and characterization methodologies which are often used to define the performance metrics. Furthermore, we outline important questions and identify emerging trends in relation to the remediation strategy towards improved photocatalytic performance and stability from halide perovskite semiconductors.

Broader context

Fossil fuel-dependent growth has led to an unprecedented rise in atmospheric CO_2 levels. This has triggered climate change which is one of the biggest global challenges of our time. A paradigm shift to renewable energy is urgently required to decarbonize the economy and ensure carbon-neutral and sustainable growth. Artificial photosynthetic systems, inspired by natural photosynthesis, have garnered tremendous interest in the spontaneous generation of value-added chemical fuels from CO_2 and water entirely from solar energy. Halide perovskites have emerged as a promising material system for photoelectrocatalysis, after their resounding success in photovoltaics. The versatile properties of halide perovskites unlock the key to facilitating many important catalytic reactions, beyond CO_2 conversion. This perspective provides a comprehensive and critical assessment of the potential of cost-competitive halide perovskite-based photocatalytic systems. We intend to focus the research community's interest on driving value-added catalytic reactions using halide perovskites. By doing so, we identify fundamental issues that require immediate attention and provide clear future directions that must be considered for this technology to become a commercial reality and have tangible impact.

1. Introduction

Fossil fuel dependent growth has led to an unprecedented rise in atmospheric CO_2 levels. This has triggered a climate emergency which has become one of the biggest global challenges of our time.[1] Therefore, a paradigm shift to renewable energy is urgently required to meet global energy demands and ensure sustainable growth in a cost-effective manner.[2] Two dominant factors are fueling the rapidly transforming renewable energy landscape – (i) a decrease in the levelized cost of electricity (LCOE) of photovoltaics,[3] and (ii) heavy reliance on fossil-based resources to generate liquid fuels for transportation and chemical feedstocks for high value synthetic chemicals in fertilizer and pharmaceutical industries.[4] While falling PV prices are favorable for ever increasing energy demands, the associated intermittency related to diurnal changes and climatic variations pose a limit to its applicability, especially in hard to decarbonize sectors such as transportation.[5] Thus, renewable technologies aiming to convert CO_2 and store energy in the form of synthetic fuels and value-added chemicals are highly desirable not only for developing alterative sustainable fuels but also for closing the carbon cycle.

Solar-driven photo(electro)catalysis systems, inspired from natural photosynthesis, enable spontaneous generation of high energy density and value-added chemical fuels from CO_2 and water, also known as artificial photosynthesis, solar fuels, and carbon-capture, and utilization (CCU).[6] The energy density (per unit weight or volume) of photoelectrochemically produced molecules is higher than those of conventionally used lithium batteries, making them suitable for long-term storage and mobility.[7] Thus, a clean, cost-competitive, and flexible alternative to current fossil-fuel based technologies is offered for sustainable intersectoral societal growth.

[a] *Imec, imo-imomec, Thor Park 8320, 3600 Genk, Belgium. E-mail: Sudhanshu.shukla@imec.be*
[b] *EnergyVille, imo-imomec, Thor Park 8320, 3600 Genk, Belgium*
[c] *Hasselt University, imo-imomec, Martelarenlaan 42, 3500 Hasselt, Belgium*
[d] *School of Materials Science and Engineering, Nanyang Technological University, Singapore 639798, Singapore. E-mail: Nripan@ntu.edu.sg*
[e] *Energy Research Institute @ NTU, Nanyang Technological University, Research Techno Plaza, 50 Nanyang Drive, Singapore 637553, Singapore*

The idea of renewably sourced chemicals from CO_2 recycling has intrigued researchers for decades, since the first demonstration of photocatalytic water splitting on a semiconducting TiO_2 surface by Honda and Fujishima[8] and later, photoelectrochemical CO_2 reduction using a p-GaP semiconductor by Halmann.[9] Since then, strides have been made in photocatalytic water splitting in terms of efficiency and scale.[10] In contrast, the progress in photoelectrochemical CO_2 reduction remained limited due to complexities associated with solvation dynamics, activation barrier, reaction kinetics (multiple electron and proton transfer processes), preferential dimerization, material stability in aqueous media and difficulties related to up-scaling. Moreover, the interference of impurities and spurious carbon signals renders unreliable quantification of product distribution from photocatalytic CO_2 reduction.[11]

Halide perovskites (HaPs) have emerged as low-cost, easy processable semiconductors with intriguing properties like long charge-carrier diffusion lengths and bandgap tunability and direct optical excitation with strong absorption coefficients ($>10^5$ cm^{-1}). With 26.54% certified power conversion efficiency,[12] HaP based solar cells have outcompeted many established thin film photovoltaic technologies in just 10 years. In parallel, the versatile properties of HaPs place them at the forefront of photocatalysis. For the first time, a HaP was exploited for conducting photocatalytic CO_2 reduction by Y.-F. Xu *et al.*, in 2017.[13] The authors utilized $CsPbBr_3$ QDs and their composites with graphene oxide for artificial CO_2 reduction in ethyl acetate solvent, where the pristine QDs demonstrated an average electron consumption rate of 23.7 μmol g^{-1} h^{-1}. Since then multiple studies have been conducted to improve the efficiency, selectivity, and stability of various HaPs in organic and inorganic solvents along with shedding light on reaction mechanisms and material degradation processes. For instance, recently, L. Ding and co-workers revealed the CO_2 reduction potential of $Cs_2AgBiBr_6$ QDs encapsulated in a metal organic framework by attaining CO production rates of 309.01 μmol g^{-1} h^{-1}.[14] However, the selectivity of these materials is still primarily limited to CO and CH_4, unlike materials such as carbon nitride that can selectively generate higher order carbon products. For example, the C_2H_6 evolution rate was 616.6 μmol g^{-1} h^{-1},[15] and the CH_3OH evolution rate was 13.9 μmol g^{-1} h^{-1}.[16] Profound advancements have been made in tailoring and employing HaPs for various redox reactions and chemical valorisation.

Sudhanshu Shukla

Sudhanshu Shukla is a senior researcher and Marie Skłodowska–Curie fellow at Interuniversity Microelectronics Centre (IMEC), Belgium. He obtained his PhD from Nanyang Technological University, Singapore in 2017. He was a visiting research scholar at Lawrence Berkeley National Laboratory (LBNL) and the University of California, Berkeley, USA (2016). His research interest includes fundamental understanding and application of novel photovoltaics and photoelectrochemical solar fuels generation.

2. Considerations and fundamental challenges for driving key photoelectrochemical reactions: there is plenty of room for perovskites

Several high energy density and value-added compounds can be targeted through photoelectrochemical reduction of

Vishal Jose

Vishal Jose is a senior researcher at the IMOMEC division of IMEC. He also holds an MSCA fellowship that will commence in September 2024. He received his PhD from Nanyang Technological University, Singapore, in 2022. Dr Vishal's key research interests include electrocatalysis, solar fuels, and electrochemical recycling technologies.

Nripan Mathews

Nripan Mathews is an associate professor and the Provost's Chair in Materials Science and Engineering at the School of Materials Science and Engineering at Nanyang Technological University (NTU), Singapore. His interest lies in the development of novel and inexpensive electronic materials through cost-effective techniques for electronics and energy conversion. These include organic–inorganic halide perovskites, metal oxides, and organic thin films. He is interested both in the fundamental properties of the electronic materials as well as their applications in practical devices such as solar cells, thin-film transistors, and memory devices.

environmental feedstocks such as water, CO_2 (hydrocarbons), and N_2 to obtain hydrogen, hydrocarbons and ammonia, respectively. For instance, CO_2 can be reduced and converted to obtain several high energy densities and value-added gaseous and liquid C_1 (such as CO, methane, methanol, formic acid) and C_{2+} (such as ethylene, ethanol, propanol, ethylene glycol) chemical products.[17] Thermodynamically, CO_2 reduction is an energy demanding reaction. The energy required to break the C–O bond is $\sim$750 kJ mol^{-1}. This is slightly higher than the electrochemical potential required for the hydrogen evolution reaction (HER) ($\sim$237 kJ mol^{-1}). However, kinetic factors related to CO_2 activation barrier, and complex multi-step reaction pathways push the energetics well above the thermodynamic limit, giving rise to electrochemical overpotential.[18] Similarly N_2 can be converted to NH_3, although it poses a higher challenge due to the high energy required to break the strong N–N bond. Standard reduction potentials (*vs.* RHE) and typical products are given below for various reactions involving electron and proton transfers:[19,20]

$$2H^+ + 2e^- \rightarrow H_2 \quad (E^{RHE} = 0.00\ V) \tag{1}$$

$$CO_2 + 2H^+ + 2e^- \rightarrow HCO_2H \quad (E^{RHE} = -0.17\ V) \tag{2}$$

$$CO_2 + 2H^+ + 2e^- \rightarrow CO + H_2O \quad (E^{RHE} = -0.10\ V) \tag{3}$$

$$CO_2 + 4H^+ + 4e^- \rightarrow HCHO + H_2O \quad (E^{RHE} = -0.07\ V) \tag{4}$$

$$CO_2 + 6H^+ + 6e^- \rightarrow CH_3OH + H_2O \quad (E^{RHE} = +0.02\ V) \tag{5}$$

$$CO_2 + 8H^+ + 8e^- \rightarrow CH_4 + 2H_2O \quad (E^{RHE} = +0.17\ V) \tag{6}$$

$$2CO_2 + 12H^+ + 12e^- \rightarrow C_2H_4 + 4H_2O \quad (E^{RHE} = +0.08\ V) \tag{7}$$

$$2CO_2 + 12H^+ + 12e^- \rightarrow C_2H_5OH + 3H_2O \quad (E^{RHE} = +0.09\ V) \tag{8}$$

$$2CO_2 + 14H^+ + 14e^- \rightarrow C_2H_6 + 4H_2O \quad (E^{RHE} = +14\ V) \tag{9}$$

$$N_2 + 6H^+ + 6e^- \rightarrow 2NH_3 \quad (E^{RHE} = 0.00\ V) \tag{10}$$

Oxidation reduction:

$$2H_2O + 4H^+ \rightarrow O_2 + 4H^+ \quad (E^{RHE} = +1.23\ V) \tag{11}$$

Therefore, the fundamental limitation arises from the overall voltage requirement imposed by thermodynamics and kinetics. Typically, the other half of the reduction reaction is generally coupled to the oxidation reaction, namely the oxygen evolution reaction (OER). From the above mentioned overpotential losses, the cumulative voltage requirement for the coupled HER–OER or the CO_2R–OER reaction exceeds beyond 1.8 V. Fig. 1a presents the typical reduction (in blue) and oxidation (in black) reactions performed at the photocathode and photoanode, respectively. Thus, the choice of anodic reaction is not merely limited to the OER. There are alternative oxidation reactions (AOR) such as – iodide oxidation, glycerol oxidation, plastic and biomass oxidation, degradation of organic pollutants, and selective organic transformation.[21] These are useful to obtain high value chemical compounds with overall less voltage requirement.

The input energy for endergonic reduction can be provided by the photocatalyst (an irradiated semiconductor in direct contact with the reactants) in the form of photovoltage. The fundamental principle behind a photo(electro)catalytic process consists of (i) efficient absorption of photons followed by the generation of electron hole pairs, (ii) carrier separation and transport to the surface, and (iii) electrochemical reduction or oxidation reaction involving electrons from the conduction band or holes from the valence band.[56] The overall photocurrent of the process can be expressed as:

$$J = J_{abs} \times \eta_{trans} \times \eta_{FE} \tag{12}$$

where J_{abs} is the photocurrent due to the absorbed photons, η_{trans} is the charge transfer (or separation) efficiency, and η_{FE} is the faradaic efficiency (catalysis process). Optimization of each of these parameters requires holistic materials optimization, interface engineering and control over surface chemistry.

Hence, the photocurrent and photovoltage are two critical parameters that determine the overall efficiency. Subsequent sections in the article describe how these two parameters can be optimized.

It is essential to consider different routes[57] that are used to accomplish HaP driven photoelectrochemical CO_2R: (1) photocatalysis (PC), (2) photoelectrocatalysis (PEC), and photovoltaic integrated PEC (PV-PEC) or buried junction PEC, and (3) tandem PEC scheme as depicted in Fig. 1b. Alternatively, PV powered electrolysis (PV-EC) is also a viable way to accomplish CO_2R through electrolysis. However, we will keep our focus on direct and integrated approaches in this perspective. A good account of the latest summary on perovskite-based PV-EC can be found in ref. 58. Recently, there has been a surge in research activities on HaPs for photo(electro)catalysis, evident from the rapidly growing trend of the publications in this field (Fig. 1c). Fig. 1d depicts a comparative view of the solar to carbon (STC) efficiency for different device architectures and material systems. It becomes clear that STC efficiencies for PEC and PV-PECs are well below 10% for most of the materials. It is straightforward to envisage above 10% STC from HaP devices, considering that comparable optoelectronic properties can be achieved for HaPs as for the III–V semiconductor (GaAs).

Inorganic metal oxides such as TiO_2, WO_3, ZnO, and α-Fe_2O_3 appeared as early adopters for photocatalytic systems, benefiting from the high electronegativity of oxygen, versatile metal–oxygen chemistry, and economic viability.[59–61] The ionic character of the bonds between the metal and oxygen atomic orbitals results in stable compounds with sufficiently large bandgaps, that typically straddle the redox potentials of various reduction (CO_2, H^+) and oxidation reactions (water, ethylene glycol, and 5-hydroxymethylfurfural). However, the wide bandgap of these materials limits the spectral range of optical absorption, and they suffer from high recombination losses due to a plethora of point defects and polaron formation, severely limiting the availability of carriers for photocatalysis.[62] Beyond oxides, transition metal dichalcogenides (TMDs) have garnered significant

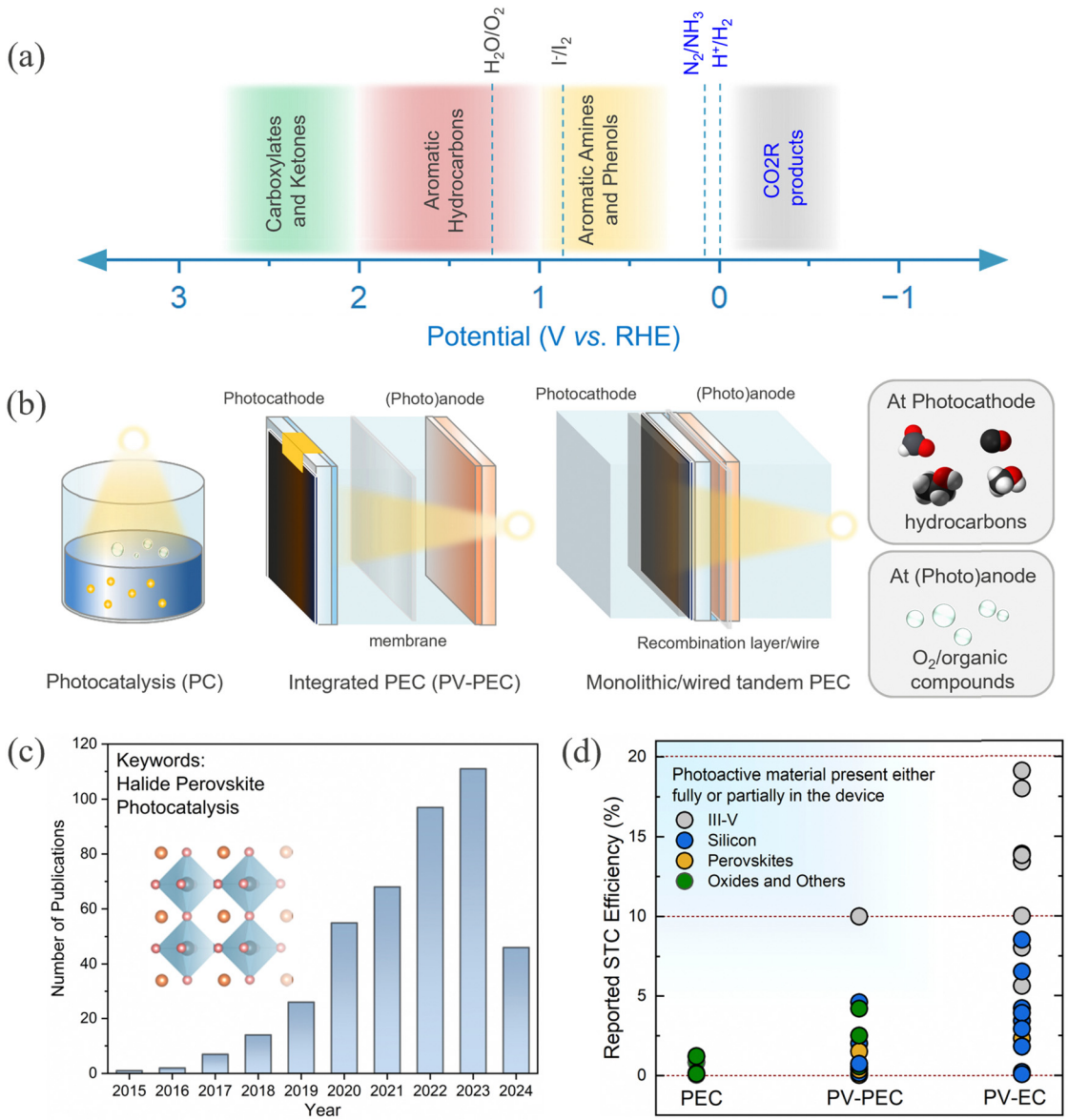

Fig. 1 (a) Common reduction and organic oxidation reactions are depicted over potential ranges.[20–23] (b) Different architecture and corresponding components of a PC, integrated PV-PEC and monolithic/wired tandem PEC device. PEC devices are configured with at least one photoelectrode (photocathode with anode or photoanode with cathode) and the integrated PEC may have a wired connected PV component. (c) Trends in publications on halide perovskite related papers on photoelectrocatalysis for the period 2015 to 2024 (source: Scopus; keyword: halide perovskite and photocatalysis, assessed on 25 April 2024). (d) Reported solar-to-carbon (STC) efficiency for different device architectures using various photoactive materials.[24–55]

attention for photocatalysis, exhibiting superior optoelectronic properties such as optical absorption, charge transport and rich defect chemistry.[63–66] However, the number of chalcogenides with sufficiently high bandgap is relatively small and, in addition, there are aggravated instability concerns related to photocorrosion in aqueous media.[65,67]

Halide perovskites (HaPs) have emerged as a promising class of materials for a wide variety of optoelectronic applications; solar cells,[68] photodetectors,[69] light-emitting diodes (LED),[70] lasers,[71] memristors,[72] and photoelectrocatalysis.[73] The rapid evolution of HaP based devices and their performance is underpinned by their exceptional optoelectronic properties such as defect tolerance, direct bandgap with high optical absorption and ambipolar transport with long-range balanced diffusion lengths. Carrier diffusion lengths, given by $L_D = \sqrt{D\tau}$, of up to 1 μm have been observed, manifesting the low defect density in HaPs. Another feature associated with the defect or disorder induced band tailing is the Urbach energy (E_u). The significantly low value of Urbach energy ($\sim$15–30 meV) is a manifestation of the superior optoelectronic quality of HaPs, compared to conventional semiconductors ($>$30 meV).[74] A gamut of unique properties of HaPs stems from its high degree of compositional flexibility and tuneability of structure, dimension, and electronic properties. The structure

of perovskites can be easily engineered, beyond archetypal $MAPbI_3$, to yield a variety of inorganic–organic hybrids and purely inorganic systems, and facile dimensional tailoring enables realization of 3D, 2D, 1D, 0D, and even mixed dimensional HaPs.[75,76] This allows band gap tuneability in a wide spectral range (from ultraviolet to near infrared) and provides control over energy band alignment for favorable energetics. Considering the above properties, HaPs seemingly satisfy the key requirements for photocatalytic devices by ensuring efficient optical absorption of photons, electron–hole pair generation, loss-less carrier transport, and seamless utilization of carriers at the interface to drive redox reactions with sufficiently high rates. However, one of the major limitations that has kept its potential untapped is their aqueous stability, and achieving product selectivity beyond C_1 (CO, CH_4) compounds. This requires more understanding of several unexplored elements related to composition, morphology, charge separation, passivation, and catalytically active sites in HaPs. The development of a HaP based photocatalyst relies on improving the optoelectronic as well as photocatalytic properties and mechanistic insights into the underlying descriptors. We discuss important factors governing the photocatalytic activity of HaPs and present methodologies to gain fundamental understanding, as shown in Fig. 2.

In this perspective, we identify the mechanistic challenges that need to be addressed and discuss potential routes to advance the field and rationalize the role that perovskites can play in the abatement of CO_2 emissions and facilitate its solar driven conversion to value-added chemicals and sustainable fuels.

3. Optoelectronic aspects of a halide perovskite based photocatalytic system

The excellent optoelectronic properties of HaPs are due to their peculiar crystallographic structure and electronic structure. The general formula for perovskites is ABX_3, where the A site is typically occupied by a monovalent organic/inorganic cation ($CH_3NH_3^+$ or Cs^+), B is a divalent metal (Pb^{2+}, Sn^{2+}), and X is a single or mixed halide anion (I^-, Br^-, Cl^-). The structure remains stable for a wide range of small (Cs^+) and large cation sizes ($CH_3NH_3^+$), governed by an empirical Goldschmidt tolerance factor.[77] The bandgap is formed primarily due to the hybridization between metal (B) and halide (X) orbitals.

The valence band maximum (VBM) is dominated by the X p characteristics (with some B site contribution) and the conduction band minimum (CBM) is derived from π antibonding of B p and X p orbitals. A cation seems to primarily behave as a spacer and does not directly contribute to the electronic structure but influences the bandgap *via* lattice deformations. Thus, the direct bandgap along with favorable p → p transition are the key factors behind high optical absorption in HaPs.[68] Notably, strong spin–orbit coupling (SOC), due to the presence of heavy metals (like Pb), has been shown to influence the optical transition and carrier lifetime due to Rashba splitting of the CBM.[78–80]

Broad spectral tunability and different bandgaps can be achieved by facile halide substitution and varying compositions of HaPs, as shown in Fig. 3a. The conduction band position for most of the perovskites is sufficiently negative relative to the

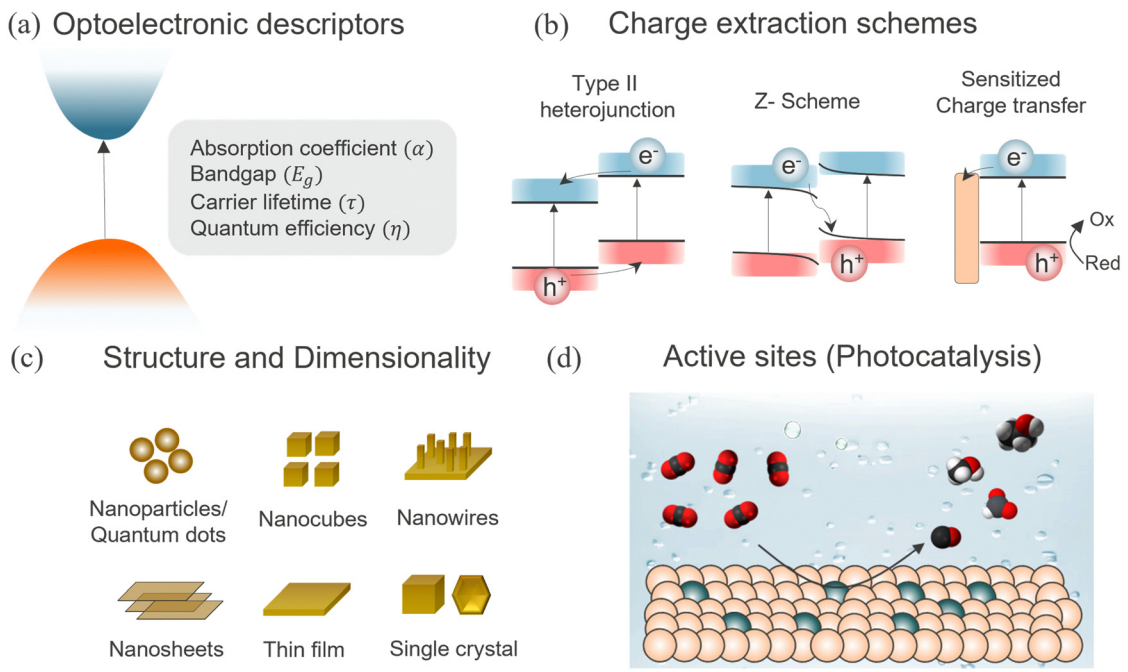

Fig. 2 Overview of the themes covered in this perspective. (a) Perovskite band structure and key optoelectronic properties, (b) different heterojunction schemes for efficient charge transfer, (c) influence of different morphology and dimensionality and (d) the role of surface chemistry in defining the catalytically active site.

redox potential of water splitting, CO_2R and N_2 reduction reaction (N_2RR),[81] providing the driving force to facilitate these reactions. The conduction band position can be varied through halide substitution to selectively match the redox potential. It is also evident that some HaPs have a valence band position positive enough to make them suitable for water oxidation and even for high value oxidation reactions like HMF and ethylene glycol oxidation.[21] HaPs are mostly investigated as photocatalysts for reduction reactions which are commonly coupled to a water oxidation reaction. The photoexcited electrons in the conduction band reduce CO_2, while the holes in the valence band are consumed in H_2O oxidation generating oxygen. Water also acts as a source of protons for hydrogenation of photocatalyzed CO_2, in addition to serving as a reducing agent.

In practice, a combination of photocatalysts is more conducive for optimum light absorption, as shown in Fig. 3b, while maintaining the necessary photochemical potential higher than the redox potential. This is generally achieved by forming heterostructures.

3.1. Photophysical and charge transfer processes in halide perovskites

Upon irradiation of light above or equal to the bandgap, photoexcited electron–hole pairs are generated and migrate to the surface primarily through diffusion. Drift transport is believed to be less important in perovskites, as the electric fields are screened by the presence of moving ions.[84] During the migration, carriers undergo various photophysical radiative and/or non-radiative recombination processes due to the presence of disorder, shallow traps, and deep defects. The lower defect density in HaPs ensures long carrier diffusion lengths, implying a reasonably high carrier recombination lifetime and mobilities. Since photoelectrochemical reactions are kinetically slow processes, the photoexcited carrier lifetime must be long enough to ensure the availability of carriers at the surface for redox reactions (Fig. 4a).[85] Thus, charge carrier lifetime (τ) is the most essential descriptor to describe the photocatalytic ability associated with its optoelectronic quality. Determination of the carrier lifetime has mostly relied on the photoluminescence (PL) based measurements. Fig. 4a shows the carrier lifetime values reported in the literature and the corresponding regime for various HaPs, deduced from photoluminescence measurements. Apart from PL, other transient techniques such as – time resolved microwave conductivity (TRMC), optical pump THz probe (OPTP) spectroscopy, transient absorption spectroscopy (TAS), transient photovoltage (TPV) and photoconductivity measurements, have also proven to be quite useful in lifetime assessment.[86–88] For instance,

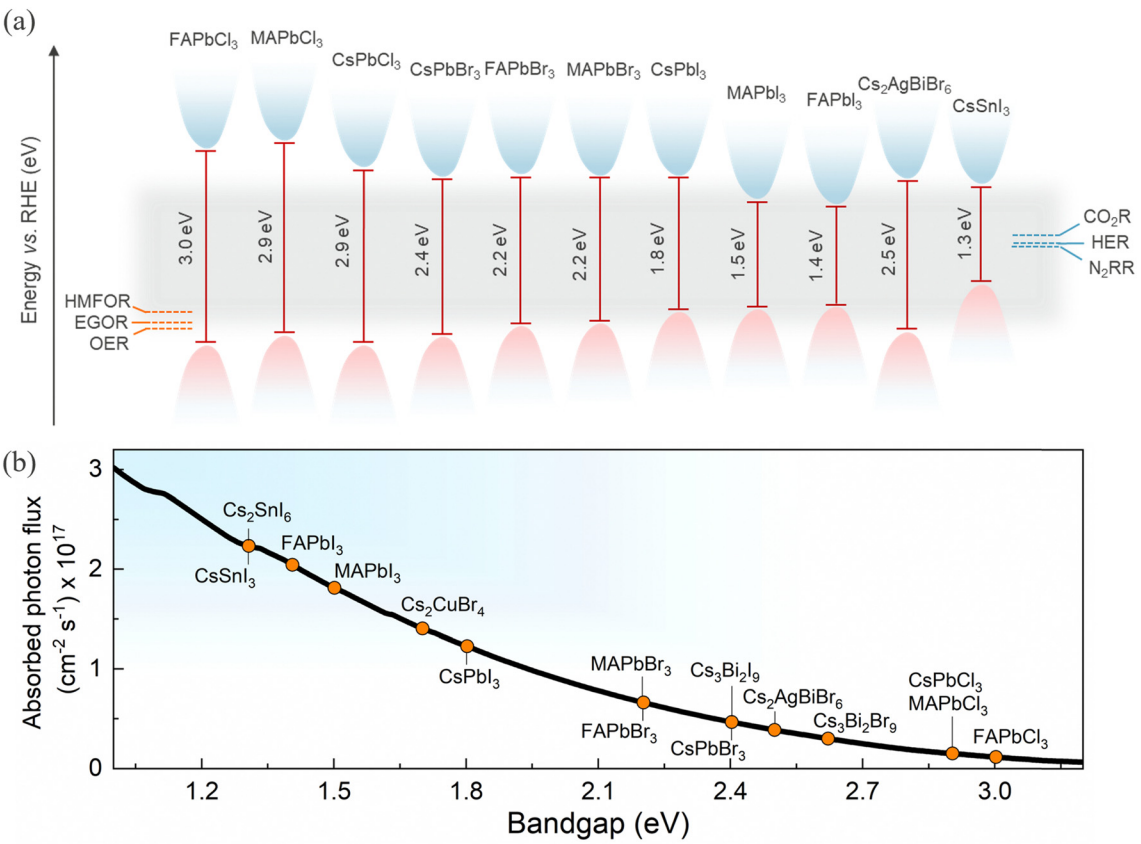

Fig. 3 (a) Valence and conduction band positions of selected HaPs with respect to relevant redox cathodic and anodic reactions.[82,83] (b) AM1.5G equivalent steady-state absorbed photon flux available for different bandgap HaPs (assuming step-function-like absorptivity) representing their light absorption ability.

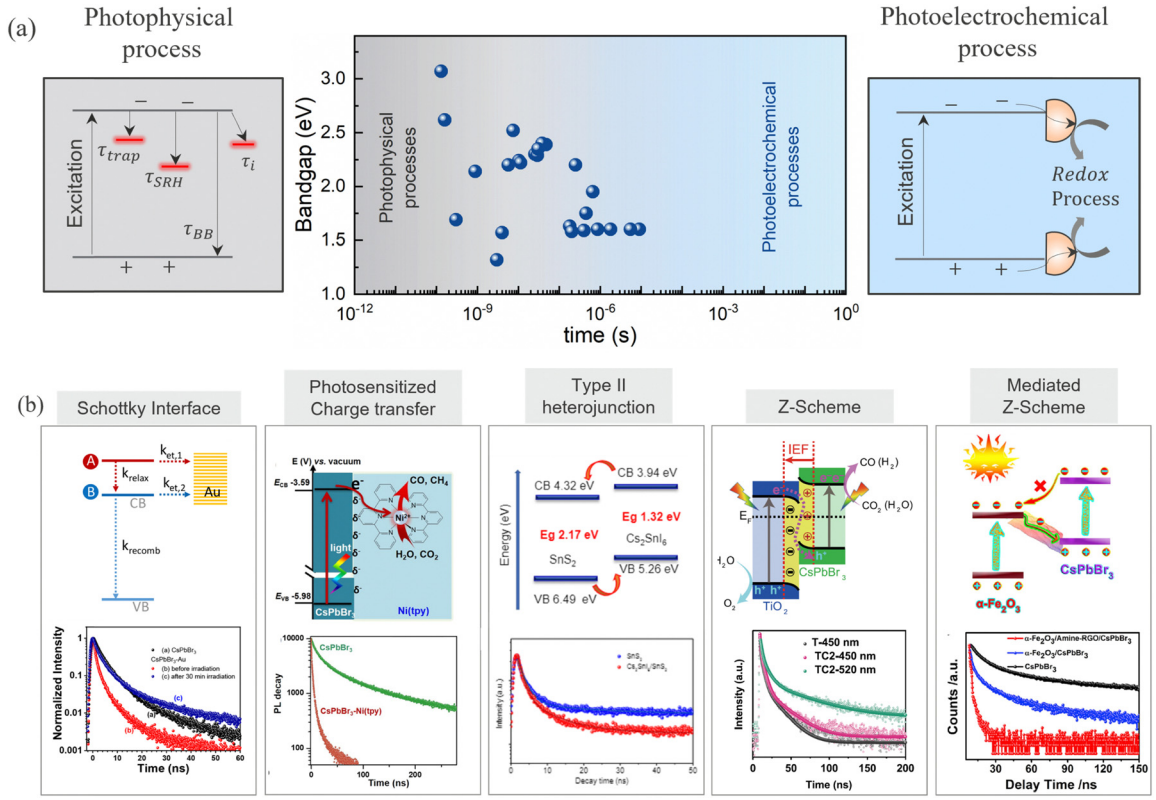

Fig. 4 (a) Charge carrier lifetimes for various HaPs derived from transient photoluminescence spectroscopy. Photophysical and photoelectrochemical regimes are differentiated based on the different timescales. The data points are taken from the literature.[91–113] (b) Heterojunction schemes utilized to separate the photogenerated charge carriers and drive photoelectrochemical CO_2 reduction from HaPs. Schottky interface, reprinted with permission from ref. 114. Copyright 2021 American Chemical Society. Photosensitized charge transfer, reprinted with permission from ref. 92. Copyright 2021 American Chemical Society. Type II heterojunction, reprinted with permission from ref. 93. Copyright 2019 American Chemical Society. Z-Scheme, reproduced from ref. 94. Copyright 2020 Nature Publishing Group. Mediated Z-Scheme, reproduced from ref. 95. Copyright 2020 Cell Press.

Chen *et al.* revealed a long carrier lifetime of up to 30 μs and 2.7 ms for $MAPbI_3$ polycrystalline films and $MAPbBr_3$ single crystals, respectively, from steady-state photoconductivity and Hall measurements.[89] Brenes *et al.* observed a carrier lifetime of 32 μs in the passivated $MAPbI_3$ thin films from TRMC measurements.[90]

Photophysical processes like – trap assisted recombination, Shockley–Read–Hall (SRH) recombination, and surface or interface recombination reduce the carrier lifetime and manifest as a change in decay dynamics of transient PL. All these processes are usually concealed in the carrier decay dynamics. While it is straightforward to deduce lifetimes from transient profiles, it is hardly possible to discern underlying physical recombination processes without fluence dependent measurements and an appropriate model.[115] The identification of the lifetime limiting process is imperative to develop focused passivation strategies and enhance the carrier lifetime. Several strategies ranging from doping and alloying,[116] nanostructuring,[117,118] bulk and passivation,[91,119–122] and dimensional tailoring,[123–125] have been demonstrated to enhance the lifetime of carriers in HaPs. Lessons from photovoltaics could be extremely useful to design passivation strategies and harness the photocatalytic activity from enhanced carrier lifetimes.

Next to long carrier lifetimes, charge carrier extraction is extremely important for efficient functioning of a photocatalytic device. Charge carrier separation is achieved through different heterojunction schemes, as shown in Fig. 4b. The common heterojunction charge transfer schemes are – Schottky junction, type II heterojunction, Z-scheme heterojunction (direct and mediated), molecular sensitization. Heterojunction layers commonly serve the dual role of passivation and carrier selective transport layer.[126–128] It is shown that despite long carrier diffusion lengths, carrier collection can be limited by unoptimized, and low mobility charge transport layers.[129] The charge transfer from perovskites reduces the carrier density within the perovskite absorber, therefore the concomitant drop in the PL intensity can act as a qualitative descriptor of the transfer kinetics. Consequently, transient PL has been exploited as a quantitative method to analyze recombination and charge transfer kinetics. This is evident from the reduction in PL lifetimes for $CsPbBr_3$/Au (Schottky),[114] $CsPbBr_3/[Ni(tertpy)_2]^{2+}$ (molecular sensitizer),[92] Cs_2SnI_6/SnS_2 (type II),[93] $CsPbBr_3/TiO_2$ (Z-scheme),[94] $FAPbBr_3/\alpha$-Fe_2O_3 (Z-scheme),[130] and $CsPbBr_3$/rGO/α-Fe_2O_3 (mediated Z-scheme),[95] heterojunctions studied in the literature, as shown in Fig. 4b. The enhanced charge separation correlates directly with the improvement in the

respective photocatalytic activities. The trend holds across a wide range of heterojunction combinations – $CsPbBr_3$ QDs/GO,[13] $CsPbBr_3$/g-C_3N_4,[131] $CsPbBr_3$/TiO–g-C_3N_4,[132] $CsPbBr_3$/MXene nanosheets ($Ti_3C_2T_x$),[133] $CsPbBr_3$/N-doped carbon dots,[134] $CsPbBr_3$ QDs/Bi_2WO_6 nanosheet,[135] $FAPbBr_3$/Bi_2WO_6,[136] $CsPbBr_3$/CdS,[137] ZnSe nanorods/$CsSnCl_3$,[138] and $Cs_3Bi_2Br_9$/g-C_3N_4.[139] Some of these benefit from an interfacial electric field that further assists in charge separation. High surface area and porous metal organic frameworks (MOFs) have also been explicitly used as charge extracting layers which are advantageous against insulating SiO_2,[140] or an inorganic/polymer matrix.[141] $CsPbBr_3$–zeolite imidazolate (ZIF) core–shell composite,[96] $MAPbI_3$ QDs/PCN-221 (Fe-based porphyrin) encapsulated structure,[97] and $Cs_3Bi_2Br_9$ and $Cs_2AgBiBr_6$ nanodots/mesoporous titania facilitated enhanced electron transfer to promote photocatalytic CO_2 reduction to CO and CH_4 respectively.[98] While lifetime changes help, the unambiguous determination of charge transfer from PL kinetics requires the knowledge of carrier injection levels. This is frequently overlooked in the measurements. Thus, fluence conditions are extremely critical to unambiguously discern decay components related to charge transfer and not due to recombination activity. Moreover, subjecting to similar light illumination conditions used during the device testing would be beneficial to gain mechanistic understanding.

Another concern is regarding the steady-state PL quenching, which is also described as a marker of the charge transfer process. However, PL quenching may also occur due to enhanced recombination at the interface and/or reabsorption effects from the heterojunction layer rather than charge transfer. Ideally, the heterojunction should maintain a high PL under open-circuit conditions (which is mostly the case) due to the passivating nature of the interface. This way steady-state PL is quite useful to screen the passivating interfaces. On the other hand, rapid PL quenching should occur when deviating from open circuit conditions *i.e.*, when the charge carriers are efficiently extracted. Considerations on energy band alignments are necessary to ensure efficient transfer of charges.

3.2. Charge separation and its utilization for catalysis

Despite a plethora of experimental demonstrations, the fundamental understanding remains unclear regarding how separated charge carriers participate in the catalytic reaction. How many separated charge carriers indeed participate in the photocatalytic reaction and determine the faradaic efficiency? How do surface traps/defects influence the surface charge and photocatalytic activity? What is the effect of charge separation on stability? These questions can be partially addressed by *in situ* and operando spectroscopic techniques such as photoluminescence, transient absorption, and impedance spectroscopy, which can provide valuable mechanistic insights with high spatial resolution.

The success of defect passivation and charge transport layers in HaPs based solar cells has not been translated to photoelectrochemical devices. *In situ* studies can provide mechanistic insights on charge transfer at the complex HaPs/electrolyte interface and determine the rate limiting step. Multilayered tandem architectures and selective co-catalyst integration should be explored to maximize charge transfer efficiency. Thus, minimization of energy loss should be considered at every interface. Recent demonstrations on the possibility of hot carrier extraction in particulate HaPs photocatalysts expand the capabilities of these materials.

4. Photocatalytic reactions on halide perovskites

4.1. Engineering morphology and dimensionality for enhanced photocatalytic performance

HaPs morphology and dimensional engineering have been shown to influence photocatalytic activity through a change in the local electronic structure induced by the surface coordination environment, catalytic reaction sites, surface charge density, binding energy of CO_2 and intermediates, and surface area. In terms of morphology, quantum confined HaP structures have been explored in photocatalysis, such as QDs (0D), nanorods/nanowires (1D), nanosheets/nanoplatelets (2D), and nano/microcrystals crystals (>100 nm, 3D).[142]

Nanocrystalline HaPs show enhanced photocatalytic activity due to their high surface-to-volume ratio and demonstrate more resilience to phase transformations. However, they tend to be less stable compared to their bulk counterparts. Specific advantages and opportunities for nanocrystalline HaPs include suppressed phase segregation, exploitation of hot carriers, and high surface area. On the other hand, charge carrier extraction is challenging in such nano dimensional systems due to the excitonic nature of the optical excitations as evidenced from high PL quantum yields (PLQY) and lower lifetimes. An additional challenge comes from charge transport limitations as many of the QDs are coated with insulating ligands. Hence, the efficiency of perovskite QD solar cells is far lower than perovskite thin film solar cells. A comparative view based on important metrics for photocatalysis for single crystals, thin films and nanoparticles is shown in Fig. 5.

Lowering the dimensionality leads to a higher surface area which is beneficial for catalytic charge transfer. A study on nanocrystal size dependence showed higher photocatalytic activity and stability for a 8.5 nm quantum confined nanocrystal, leading to a longer PL lifetime of 9.7 ns.[143] Two dimensional (2D) layered structures provide better conducting pathways for charge transfer due to the large interfacial area. For instance, Jiang *et al.* fabricated a heterojunction from $CsPbBr_3$/Bi_2WO_6 2D sheets for CO_2 reduction,[144] where a higher interface area of 2D sheet led to a 5-fold increase in CO_2 conversion yield compared with bare $CsPbBr_3$ nanosheets (Fig. 6a–c). Functionalization of a co-catalyst can further help in boosting the photocatalytic activity. However, maintaining the structural integrity of the co-catalyst on the support and avoiding precipitation during the photocatalytic reaction is extremely daunting.[145] The improvements from nano sizing, although seemingly obvious, need to be rationalized for long term performance. Research work from Zhu *et al.* critically assessed the viability of $CsPbBr_3$ nanoparticles with different sizes (4 nm to 24 nm) for organic transformation,

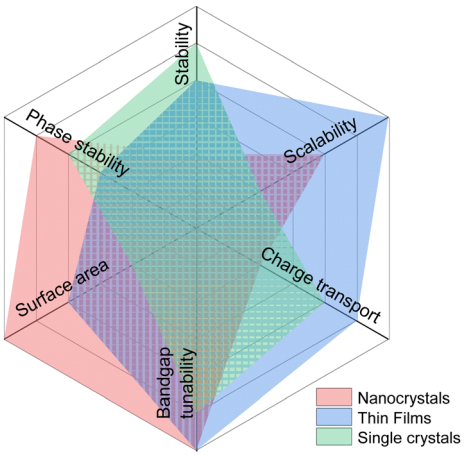

Fig. 5 Radar chart depicting the comparison of different metrics for nanocrystals, thin films, and single crystals HaP-based photocatalytic systems.

as shown in Fig. 6d and e. They observed that while faster photocatalytic activity is observed initially for smaller HaP nanocrystals, the overall yield remained less than larger nanocrystals in long term operation[146] (Fig. 6f).

4.2. Exploitation of different crystal shapes and facets

The synthesis of different shapes of halide perovskite nanoparticles offers new opportunities in photocatalysis. Reasonable success has been achieved in synthesizing shape-controlled nanoparticles, such as facile room temperature synthesis of $CsPbX_3$ nanoparticles.[147] Since halide perovskites have long electron and hole diffusion lengths, the anisotropy in the crystal structure can lead to different electron and hole migration pathways which can help in spatial decoupling of the reduction and oxidation reactions. Li *et al.* have showed migration of holes and electrons to the edge (100) and (006) basal facets, respectively, on $Cs_3Bi_2I_9$ hexagonal prisms, using Co^{2+} (for oxidation) and Pt^{4+} (for reduction) as redox probes, as shown in Fig. 7a.[148] Different atomic arrangements on crystal facets dictate the surface energy and the interaction with the reaction environment. Selective functionalization of co-catalysts over crystal planes that have reduced kinetic barriers for photocatalytic CO_2 reduction is highly interesting. This strategy has recently showed quantum efficiency approaching 100% for photocatalytic water splitting reaction by selectively functionalizing Rh/Cr_2O_3 at (100) and CoOOH at the (110) facet of the $SrTiO_3$-Al nanoparticle as a HER and OER co-catalyst, respectively.[149] Similarly, taking advantage of the crystallographic anisotropy, pseudo type-II facet selective $CsPbBr_3$–sulfobromide $Pb_4S_3Br_2$ epitaxial heterostructures have been demonstrated to improve the catalytic activity (Fig. 7b).

In a recent study, albeit for solar cells, it is shown that the (111) facet dominated $FAPbI_3$ film is more stable against moisture and phase transition, which the authors attributed to the reduced chemisorption/interaction strength of water molecules on the (111) facet compared to the (100) facet that

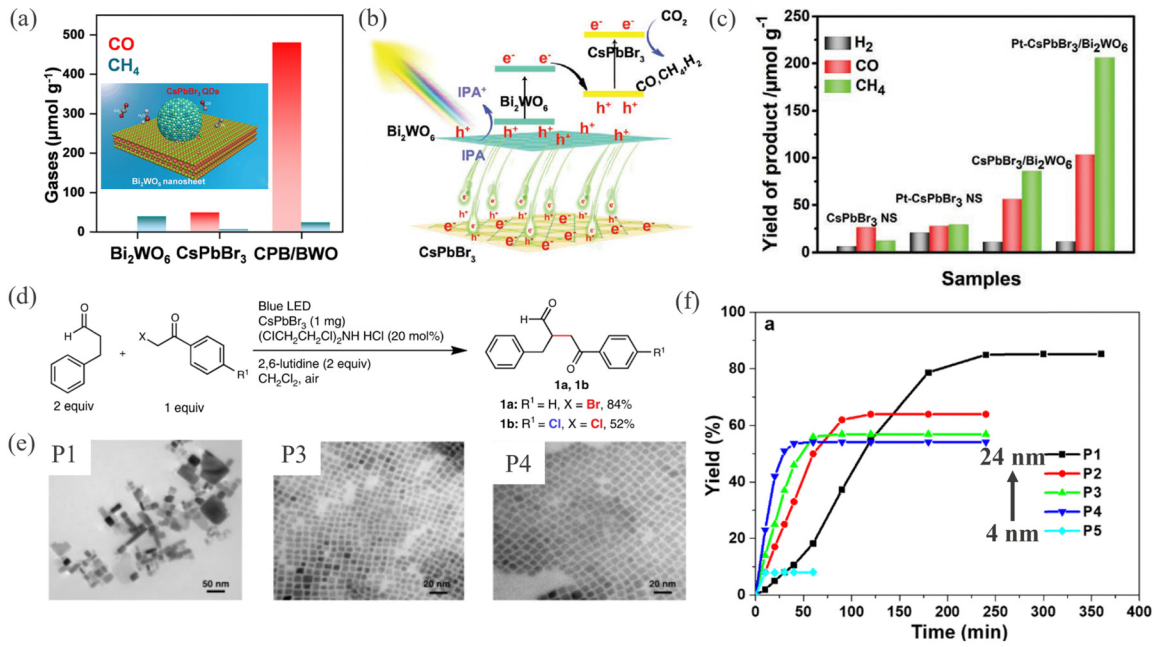

Fig. 6 (a) Product yield during CO_2 photoreduction/H_2O photooxidation over 0D/2D $CsPbBr_3/Bi_2WO_4$ and its individual components. The inset shows a schematic illustration of the $CsPbBr_3$ zero-dimensional (0D) nanocrystals. Reprinted with permission from ref. 135. Copyright 2020 American Chemical Society. (b) Conceptual band diagram of the 2D/2D heterojunction depicting the Z-scheme and charge carrier dynamics. (c) Product yield rates during photocatalytic CO_2 reduction/isopropyl alcohol oxidation over the 2D/2D heterostructure system and its individual components. Reproduced from ref. 144. Copyright 2020 Wiley. (d) Organic transformation reaction and the resulting product. (e) Transmission electron microscopy images of various sizes of $CsPbBr_3$ nanocrystals as photocatalysts. (f) Percent yield of product over time for $CsPbBr_3$ nanocrystals as a function of nanocrystal size (P1, P2, P3, P4 and P5 refer to 24 nm, 14 nm, 9 nm, 6 nm, and 4 nm respectively). Reproduced from ref. 146. Copyright 2019 Nature Publishing Group.

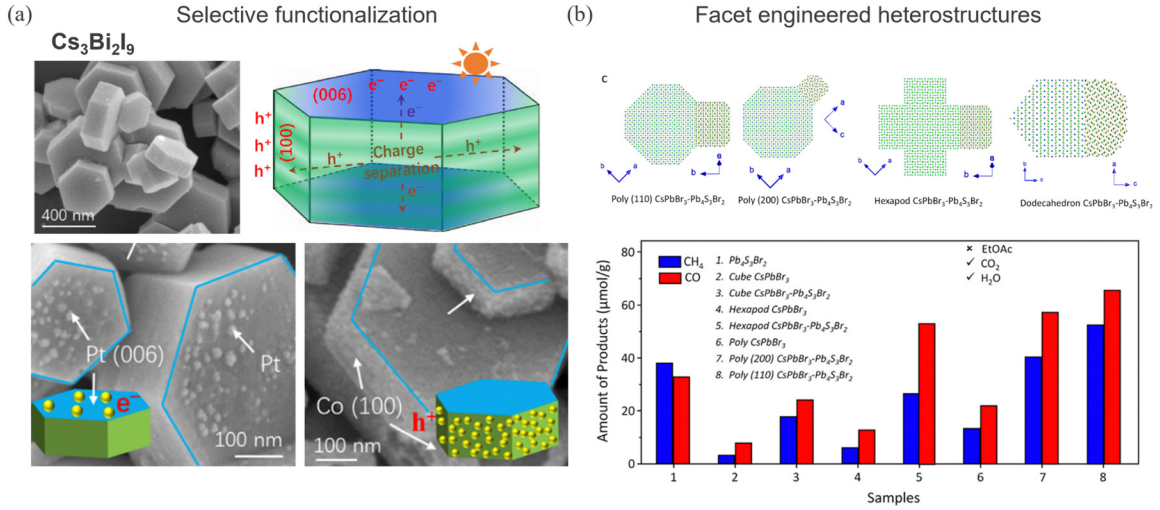

Fig. 7 (a) Anisotropic charge transport pathways leading to distinct interaction at (100) and (006) facets of $Cs_3Bi_2I_9$ hexagonal prisms. Reprinted with permission from ref. 148. Copyright 2022 American Chemical Society. (b) Atomic models of $CsPbBr_3$–sulfobromide $Pb_4S_3Br_2$ heterostructures of different shapes: rhombicuboctahedronin, hexapods, and dodecahedron nanostructures. (bottom) Product distribution after 2 h of photocatalytic reaction for different heterostructure shapes under CO_2-saturated H_2O vapor. Reprinted with permission from ref. 150. Copyright 2022 American Chemical Society.

is predominant is conventional thin films.[151] These studies clearly suggest the importance of facet engineering in achieving high performing and stable photocatalytic devices.

4.3. Activation and manipulation of catalytically active sites

Catalytically active sites are essential for the desired reduction and oxidation activity. The intrinsic activity of the active sites depends on inherent electronic structuring and surface atomic arrangements that affect the adsorption and desorption of reactive intermediates. Exposing active sites over the surface and enhancing their accessibility for the reactants could modulate photocatalytic performance. Apart from poor stability in electrolytes, HaP also suffers from a lack of highly active sites for the desired reactions.[152] Various strategies, such as morphology engineering, surface/interface structuring, heterojunction construction, encapsulation methodologies, and pairing co-catalysts, are explored to enhance the activity of HaP photocatalysts. For instance, Y.-F. Xu *et al.*, reported the development of $CsPbBr_3$ nanocrystal/palladium nanosheet ($CsPbBr_3$NC/Pd NS) composites for improved photocatalytic CO_2 reduction in water vapor.[153] This study revealed that even though the pristine $CsPbBr_3$ nanocrystals displayed activity for CO_2 reduction, the performance could be significantly enhanced by integrating with Pd nanosheets (photoelectron consumption rate increased from 9.86 to 33.9 μmol g^{-1} h^{-1}). This performance enhancement could be stemmed in fact from the creation of metal/semiconductor Schottky contact between Pd NS and $CsPbBr_3$ NCs that accelerates the charge separation and transfer properties along with exposure of catalytically active Pd sites.

Using the binding sites on HaP to immobilize catalytically active species can assist in achieving a high reaction activity of HaP-based hybrid photocatalysts. For example, Z. Chen and co-workers stabilized a $[Ni(terpy)_2]^{2+}$(Ni(tpy)) metal complex on inorganic ligand-capped $CsPbBr_3$ NCs to form a $CsPbBr_3$–Ni(tpy) hybrid photocatalyst.[92] Apart from providing active Ni(tpy) catalytic centers, the metal complexes also served as electron sinks by accepting photoexcited electrons from HaP nanocrystals and thus suppressing electron–hole recombination. Consequently, $CsPbBr_3$–Ni(tpy) hybrid photocatalyst yielded 1724 μmol g^{-1} (CO/CH_4) in the reduction of CO_2, which is about 26 times higher than the yield achieved by pristine $CsPbBr_3$ NCs. In another work, L.-Y. Wu *et al.*, encapsulated $MAPbI_3$ perovskite QDs in the pores of a Fe-porphyrin based metal organic framework (PCN-221(Fe_x)) through a sequential deposition procedure.[97] Utilizing steady-state and time-resolved PL measurements, it was revealed that, due to close contact of absorber and catalysts, photogenerated electrons from $MAPbI_3$ QDs can easily be transferred to catalytically active sites of Fe porphyrins and thus enhance the charge separation efficiencies and activity of the resulting hybrid photocatalyst. Furthermore, metal–organic framework structures were also found to improve the stability of $MAPbI_3$ QDs in water-involved photocatalytic systems. Following these effects, the optimized $MAPbI_3$@PCN-221(Fe_x) exhibited a CO_2 reduction yield of 1559 mmol g^{-1} (CO (34%) and CH_4 (66%)) with high stability (linear productions over 80 hours). The exploration of such strategies seems to improve the effectiveness of HaP-based photocatalysts in CO_2 reduction. However, more efforts are required to enhance the activity-stability of these newly emerged photocatalysts.

Surface active sites should be optimized in terms of their density, accessibility, and intrinsic activities. Given that the fundamental understanding of catalytic mechanisms is still limited, *in situ* characterization techniques and DFT-based calculations on surface energies with considerations on intermediates should help to achieve better optimizations. For instance,

the defective states in materials can be trap sites for carriers, leading to an increased rate of electron–hole pairs recombination. On the other hand, defective sites could come with increased intrinsic activity, facilitating better reaction rates. Therefore, systematic analysis and detailed investigations based on *in situ* and theoretical studies help exploit the materials to off-limits. *In situ* analysis also assists in revealing the dynamic surface reconstruction of catalysts during the actual testing. Further augmentation with advanced machine learning algorithms can help in rationalizing and elucidating the catalytically active sites *via* high-throughput complex calculations of site-specific reactant binding energies and reaction intermediates.

4.4. Product selectivity for CO_2R products

The product selectivity primarily depends on the surface electronic states which govern the CO_2 activation/adsorption, catalytically active sites, and intermediate adsorption/desorption properties. Also, the availability of surface charges dictates the reaction pathways. Evidently, it is difficult to achieve reduction products that involve a higher number of electrons at the surface, such as CH_3OH and other C_{2+} products. CO and CH_4 are the major CO_2 reduction products for HaPs. The product yield for various HaPs is shown in Fig. 8a and b and compared against other photocatalysts for CO_2 reduction. There is no report on methanol or higher order C_2 product yet. Success in improving CO and CH_4 production has been achieved through different heterojunction schemes, morphology, compositional and dimensional engineering, as discussed above. The relative distribution of CO and CH_4 from different heterostructures is shown in Fig. 8c. Mechanistic and theoretical insights on CO_2 activation and adsorption energy of intermediates, and proton coupled electron transfer reaction (PCET) is lacking for HaPs, contrary to oxide perovskites.

Sheng *et al.* exploited the concept of frustrated Lewis pairs (FLP) to achieve efficient dissociation of H_2 and CO_2 reduction on Pb-free $Cs_3Bi_2Br_9$ and Cs_2CuBr_4 quantum dots.[99,101] Utilizing *in situ* diffuse reflectance infrared Fourier transform spectra (DRIFT) and density functional theory (DFT) calculations, the authors show that the surface catalytic sites can be regulated *via* bromine modulation and spontaneous polarization effect due to Cu-d band properties in $Cs_3Bi_2Br_9$ and Cs_2CuBr_4 respectively.

The estimation of the energetic barrier and binding strengths of key intermediates such as CO*, COOH* and CH_4* species on perovskite surfaces are critical to alter and design surfaces that can steer the reaction kinetics in different hydrogenation pathways. Studies combining *in situ* experiments and theory can be extremely valuable to achieve breakthroughs in the field.

5. Improvements in stability enabling advanced photoelectrochemical devices

Poor stability of perovskite based photoelectrodes in PEC type devices limits their potential due to the reduction in the photovoltage output over time. The photovoltage loss incurred due the degradation reduces the solar-to-fuel conversion efficiency. Both intrinsic (ion migration, defects and traps, phase instability) as well extrinsic environmental stresses act to trigger or accelerate degradation. Adequate bulk and surface passivation schemes through additive engineering, molecular passivation, and barrier layers have drastically improved the stability of perovskite devices with minimal photovoltage loss.[167–169] Additionally, applying an external encapsulation layer and/or changing the chemical environment improves the operational stability of perovskite photoelectrodes in aqueous media, providing an extended window to drive various reduction and oxidation reactions.

5.1. Perovskite based photocathodes for reduction reactions

The most widely explored $CsPbBr_3$ had an average carrier lifetime in the range of 1–50 ns, which is significantly lower than the HaPs used in best performing solar cells. This is due to the aqueous instability issues associated with HaP compositions used in solar cells. The chemical bonding in HaPs is highly ionic in nature, which causes instability in polar solvents and liquid electrolytes. This is usually mitigated by exploiting dynamic precipitation-solubility equilibrium in HX acid solution,[170] or using purely organic or mixed aqueous–organic solvents.[135,144] Therefore, alternative oxidation of organic compounds is advantageous both with regards to stability and energetics. Ethyl acetate, isopropyl alcohol and benzyl alcohol have been used for oxidative half reactions. This provides an opportunity for synthesizing a wide range of value-added chemicals. However, the practical and economic benefit of utilizing these chemicals must be assessed in advance.

Additive engineering and site-specific molecular passivation routes have also been quite successful in achieving long term stability of perovskites in PV devices while simultaneously addressing the ion/halide migration issues. Encouraging device modifications have been proposed to make them stable in different photoelectrochemical environments. As an example of an integrated system, Liang *et al.* demonstrated carbon encapsulated $MAPbI_3$ perovskite solar cells sealed by an electrode integrated with a catalyst layer for photoelectrochemical water splitting.[171] Recently, direct integration of a catalyst on photocathode/photoanodes has been possible, thanks to a passivating and conductive carbon layer.

Fehr *et al.* showed solar driven water splitting from a mixed cation $Cs_{0.05}FA_{0.85}MA_{0.1}Pb(I_{0.95}Br_{0.05})_3$ (photocathode) and $FA_{0.97}MA_{0.03}PbI_3$ (photoanode) perovskite solar cell directly integrated with a carbon electrode with an overall STH efficiency of 20.8%.[172]

For CO_2 photoelectrochemical reduction, Andrei *et al.* demonstrated the success of a carbon encapsulation approach to fabricate a monolithic triple cation $(CsFAMA)PbI_{3.2}Br_{0.66}$ based perovskite–$BiVO_4$ tandem PEC as a standalone system for CO_2 reduction (see Fig. 9a).[29,173,174] Carbon encapsulation provides a distinct avenue to extend the applicability of wider perovskite compositions in photocatalysis. In addition to carbon, Field's metal (FM) and metallic foils are also used to enhance electrical conduction and stability. For example,

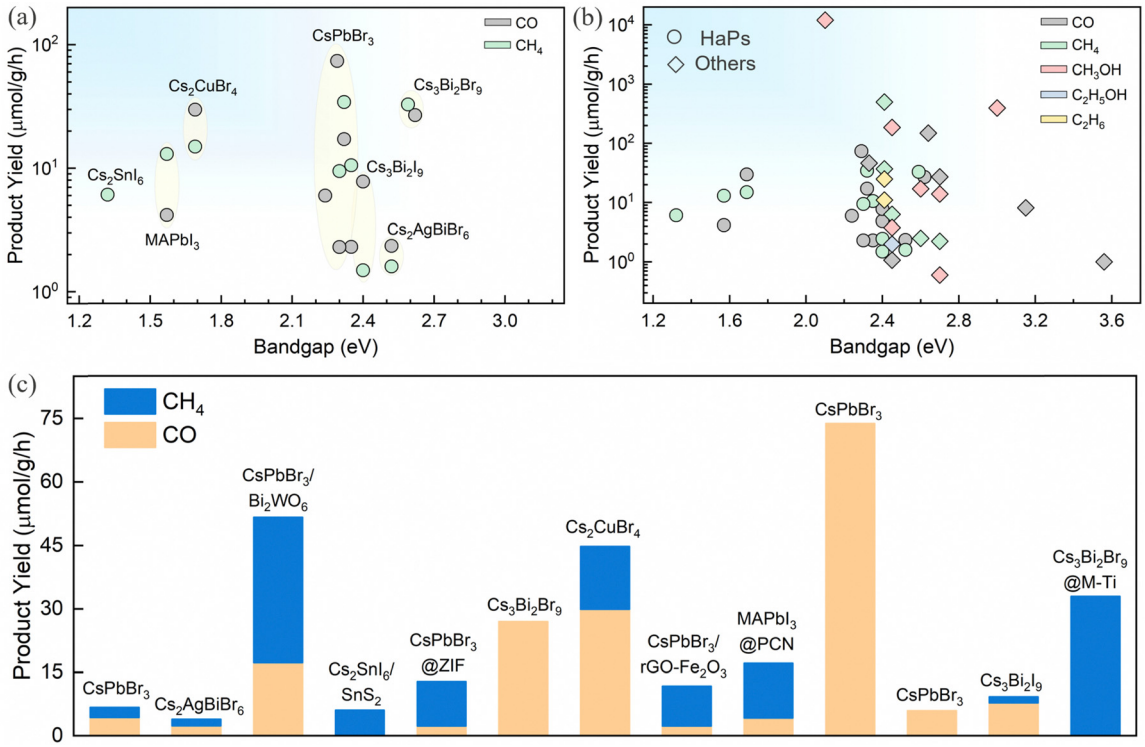

Fig. 8 (a) Product yield during photocatalytic CO_2 reduction for various perovskites, (b) comparison of products and their respective yield for HaPs and other semiconductors,[16,131,154–166] and (c) product distribution from different perovskites and perovskite heterojunctions.[13,93–101,109,111,144]

Tayyebi *et al.*[175] and Choi *et al.*[176] have demonstrated ammonia and hydrogen production respectively, from FM and metallic layer protected perovskite photocathodes, as shown in Fig. 9b and c. In this way, multi-layer protective layers, also serving as charge transport layers, have been successfully applied to drive different redox reactions (CO_2, nitrate, and water reduction) at high photocurrent density ($\sim$20 mA cm^{-2}). The coupling of alternative oxidation reactions such as glycerol and lignocellulosic biomass has opened a new paradigm in this direction.

5.2. Perovskite based photoanodes for oxidation reactions

Carbon encapsulation is not merely limited to reduction reactions but extended to perovskite photoanodes to drive oxidation chemistry. Excellent progress has been made in driving oxidation reactions from carbon encapsulated perovskite photoanodes. Mesoporous carbon protected $FAPbBr_3$ based photoanode demonstrated 8.5% STH efficiency, surpassing the performance achieved from analogous photoanodes such as $BiVO_4$, Fe_2O_3, TiO_2, WO_3, and Ta_3N_5.[177] Poli *et al.* utilized an Ir-catalyst embedded bilayer of graphite sheet and mesoporous carbon electrode protected inorganic $CsPbBr_3$ photoanode for water oxidation.[178] Stability and activity can be further improved through modulating surface chemistry and catalyst engineering. Depending on the electrochemical response of organic ligands and metallic catalysts, the redox ability of HaP-based materials can be tuned to yield value-added compounds with reduced energy input.

Recently, Zhu *et al.* have achieved remarkable stability of 210 h for water oxidation in aqueous electrolyte through encapsulating with electrocatalytically active glassy carbon and boron doped diamond sheets containing an earth abundant NiFeOOH catalyst.[179] A similar catalyst has been integrated into a high performing $FAPbI_3$ based photoanode to realize an impressive 8.5% solar-to-hydrogen (STH) efficiency on scaled-up 123 cm^2 mini modules.[180] Recent demonstrations on heterojunctions based on conjugated polymers with metal sulfide (Sb_2S_3),[181] metal oxide (Mo:$BiVO_4$),[126] and metal nitride (Ta_3N_5)[127] can be used as a basis to develop a perovskite photoanode with carrier extraction efficiency. Beyond water oxidation, few studies explore perovskite photoanodes for alternative oxidation reactions such as iodide oxidation and organic transformations for environmental remediation. The iodide oxidation reaction (IOR) has a thermodynamically lower energetic requirement and is kinetically more favorable than the OER. Yun *et al.* have developed a Co–Ni_2S_3 catalyst embedded in a carbon matrix and integrated this into a standard n–i–p perovskite solar cell stack to realize photoanodes for the IOR. Fig. 10b shows the photoanode device configuration and corresponding voltammogram with and without catalyst. The protected photoanode stack yielded a STH efficiency of 11.45% along with a stable 25 h of continuous operation.[23] Climent *et al.* demonstrated a reversible photoelectrochemical transformation of benzyl alcohol (BzOH) to benzyl aldehyde (BzCHO) and *vice versa* using a selective charge transfer scheme, *i.e.* TiO_2/$CsPbBr_3$ for oxidation and NiO/

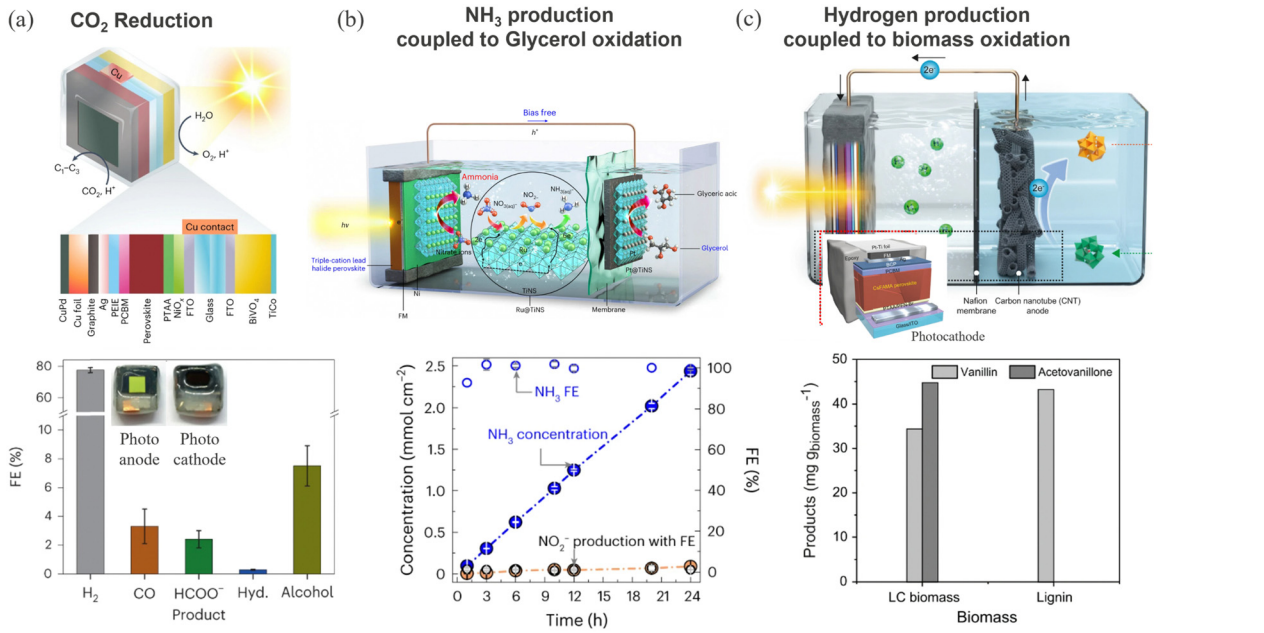

Fig. 9 (a) Schematic representation of a wireless standalone $BiVO_4$–perovskite artificial leaf like device and corresponding faradaic efficiency of various products after photocatalytic CO_2 reduction. Reproduced from ref. 173. Copyright 2023 Springer Nature Limited. (b) Schematic of the perovskite photocathode-based PEC cell used for NH_3 production. The bottom graph shows the amount of NH_3 generated for Ru@TiNS/Ni/perovskite photocathode – Pt@TiNS anode device for simultaneous nitrate reduction and glycerol oxidation. Reproduced from ref. 175. Copyright 2024 Springer Nature Limited. (c) Schematic of the perovskite PEC device for hydrogen generation at the photocathode and biomass oxidation at the anode. The bottom figure shows the production of vanillin and acetovanillone from lignocellulosic biomass, lignin, hemicellulose, and cellulose oxidation. Reproduced from ref. 176. Copyright 2022 Springer Nature Limited.

$CsPbBr_3$ for reduction.[182] The same group later extended the approach to drive the oxidation of organic pollutant such as 2-mercaptobenzothiazol (MBA) using Al_2O_3 protected $CsPbBr_3$ photoanode, as shown in Fig. 10c.[183] The efficiency of the process was further enhanced by externally powering the PEC device with a perovskite PV module.

6. Emerging concepts

While the vast majority of perovskites remain unexplored for photocatalytic application, high-throughput combinatorial screening and DFT augmented machine learning provide immense opportunities to discover stable and catalytically active perovskite compositions. Notable efforts are already being made in this direction to discover unique perovskite compounds for specific optoelectronic devices.[184–187] The optoelectronic and photocatalytic performance descriptors discussed above can guide in refining the compositional library. Advance computational methods can also help in understanding the complex and multistep photoelectrocatalysis process involving various interdependent parameters such as charge transfer, CO_2 activation, catalytic sites, reaction intermediates and competing reactions. In a recent attempt, Caruso *et al.* demonstrated the importance of choosing the correct descriptor for optimizing photocatalytic property. They combined machine learning models with the DFT and found that Zn^{2+} metal substitution at the B-site in the $Cs_2AgBiBr_6$ perovskite enhances the photoactivity due to the optimum electronic structure, especially the d-orbital configuration (d^{10}).[188] The vast library of compositionally feasible perovskite compounds remained explored. The rapid rise in the computation capabilities to screen, predict and rationalize materials properties has opened new avenues to discover stable and non-toxic perovskite or perovskite inspired compounds targeted for specific photoelectrochemical processes. Moreover, the accelerated testing platforms, also known as the laboratory of the future, can be a powerful tool for rapid screening of compositionally and operationally stable compounds. Expanding the scope of reactions from reduction to alternative oxidation reaction is gaining interest to cover wider aspects of photoelectrochemical transformations. It is important to recognize that specific HaPs might be more suitable for certain reactions and testing conditions (pH, temperature, and irradiation *etc.*).

7. Outlook and future directions

Despite significant milestones achieved for optoelectronic devices (photovoltaics, photodetectors, lasers, LEDs, *etc.*), the full potential of halide perovskites remains untapped for photocatalysis application. The photochemical performance and stability are far from its practical usage. In this perspective, we have emphasized fundamental concepts and examined key advancements propelling halide perovskites for photocatalysis. Promising paths are identified for future advancements and valorization of perovskite based photocatalytic systems.

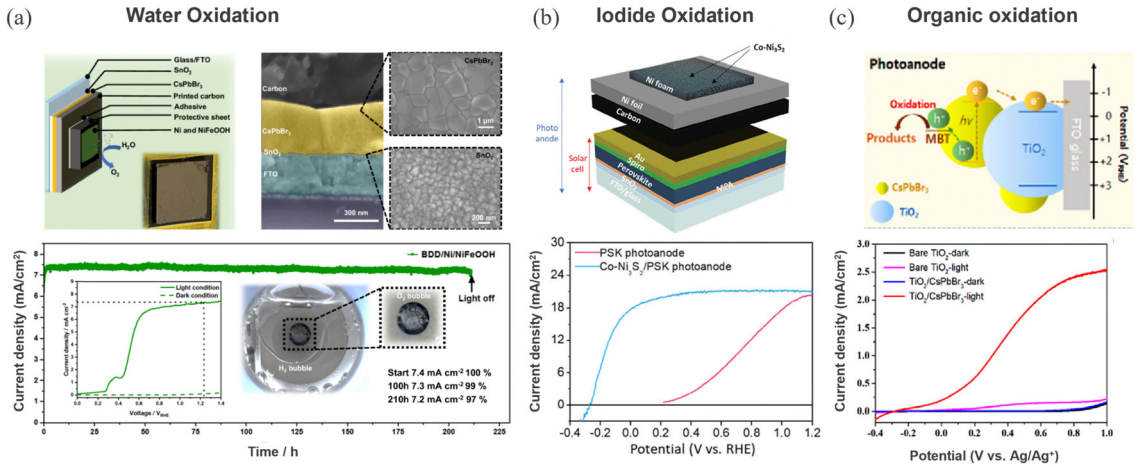

Fig. 10 (a) Water oxidation: $CsPbBr_3$ photoanode protected with GC/Ni/NiFeOOH and corresponding cross-sectional and top-view SEM micrographs of the device stack. The bottom shows the device stability testing at +1.23 V_{RHE} under 1 sun illumination. The inset shows the voltammogram under 1 sun (solid line) and in dark (green dashed line) and a photograph of the photoanode under operation showing the evolved O_2 bubbles. Reproduced from ref. 179. Copyright 2024 Springer Nature Limited. (b) Iodide oxidation: device structure of the perovskite photoanode showing Co–Ni_3S_2/Ni foam/Ni foil/carbon powder stacked on a solar cell structure and the corresponding voltammogram under 1-sun illumination in 0.5 M KPi electrolyte containing 0.5 M KI. Reproduced from ref. 23. Copyright 2024 Wiley. (c) Organic oxidation: perovskite photoanode based PEC cell for MBE oxidation and below shows the LSV scans of the photoanodes in 0.1 M tetrabutylammonium hexafluorophosphate (Bu_4NPF_6) in dichloromethane (DCM) with 0.05 M MBT. Reprinted with permission from ref. 183. Copyright 2023 American Chemical Society.

(i) Targeting stable compositions and measurement conditions

Stability of the photoelectrodes is one of the biggest challenges faced in a photoelectrochemical process. To date, archetypical $MAPbI_3$ and wide bandgap $CsPbX_3$ perovskite compositions are the most widely explored photocatalytic processes. Screening of a large number of compositions with suitable bandgaps for both reduction and oxidation reaction can accelerate the development of interesting candidates and help in identifying which composition modifications lead to higher stability. With rapidly advancing materials development initiatives, there is an urgent need for a perovskite materials database, combining theory and experiments, specific for photoelectrochemical processes. This will also lead to the discovery of more robust, stable, and Pb-free compositions suitable for photocatalysis. There is a need to critically define the optimum reaction conditions such as – pH, temperature, and consider the viability of driving complete reaction at lower overpotentials with high production rate. External strategies such as facet engineering, novel protective coatings (oxide/metal/organic) and structural engineering approaches (like core–shell structures, MOF-based encapsulation, *etc.*) must be developed and explored to stabilize perovskites in electrolytes. Apart from developing protective materials, their deposition/coating strategies, growth mechanisms, effects on perovskites, and photoelectrochemical activity should be investigated and understood in-depth.

(ii) Better charge transfer schemes for enhanced photocurrent

Leveraging upon the successful passivation schemes used for aqueous water splitting and CO_2 reduction, further improvement in performance can be achieved through better charge collection. In this regard, alternative heterojunctions beyond conventional electron and hole transport layers need to be developed, particularly Z-scheme configurations. Z-scheme with an optimum combination of bandgap (1.6 eV, top cell and 1.1 eV bottom cell) not only enhances the light absorption but also enhances the photo reduction/oxidation ability. Developing high surface area textured surfaces can further enhance the charge collection with better light management.

(iii) Driving alternative reactions for value added chemicals

Due to the instability in water based aqueous media, perovskites are stabilized in alternative media, mainly, saturated hydrohalic acid (HX; HI, HBr) solutions. The resulting products from HX splitting, I_2 and Br_2, are useful products for hygiene and energy industries. Moreover, exploring alternative anodic oxidations to the OER is desirable to lower the PEC energy requirements. Halide oxidation is thermodynamically more favorable over the OER and requires less kinetic overpotential due to two electrons being involved in the reactions compared to four electrons for water oxidation. By coupling alternative reactions such as oxidation of biomass derived organic compounds (lignin, glucose, furfural, 5-hydroxymethyl furfural; HMF, glycerol, *etc.*) and chemical wastes (polyethylene terephthalate; PET, glyceric acid, wastewater remediation), several high value chemicals such as FDCA, dimethoxydihydrofuran, vanillin, and glycolic acid, *etc.* can be achieved as byproducts of these reactions. This approach has significant potential in reducing the energy input of the paired electrochemical process, enhancing the overall techno-economic viability, and maximizing the return of energy investments. The integration

of high selectivity metal complex (Ni, Fe, Ru, and Ir) based molecular catalysts and (bi-) metallic (Au, Pt, and Pd) co-catalysts is a promising direction to enhance the functionality of the perovskite photocatalysts. The future endeavors must eventually go beyond the above and cover additional important reactions like seawater splitting and wastewater treatment.

(iv) Towards higher order carbon compounds

A higher photovoltage is desirable to overcome overpotential losses associated with photoelectrochemical CO_2 reduction. Inspiration from photovoltaic architectures might be useful to engineer novel integration methods enhancing charge extraction and stability. The high photovoltage from encapsulated and integrated perovskite PEC devices has shown promising results for unbiased standalone operation. Semitransparent perovskite PV devices can provide extra photovoltage without compromising the total photon flux. Next, overcoming mass transport limitations associated with CO_2 electrolysis, an integrated perovskite device with flow reactor and catalyst loaded gas diffusion electrode (GDE) flow reactors will pave the way for a standalone PEC device at high current densities. Surface reaction kinetics can be tuned by changing adsorption strengths of the intermediates. Advanced *in situ* characterization tools such as synchrotron-based techniques, X-ray scattering and photoelectron spectroscopy are helpful in identifying surface adsorbates and catalytic sites. Moreover, observation of catalytic transient states and charge transfer processes using ultrafast infrared and pump–probe spectroscopy bring exciting opportunities to understand the physical origin of the electrochemical processes at the perovskite surface.

(v) Scalability challenges

From a practical perspective, the scalability aspects should be considered in the beginning itself. The facile low temperature synthesis position perovskites in a favorable scenario to develop large scale processes compared to other photocatalysts, especially oxides. While nanoparticle photocatalysts show great promise, they are confronted with scaling issues. The development of thin film artificial leaf like devices is excellent in this regard while keeping the fundamental features of nanoparticles and even single crystals intact. Device scalability depends also on optimizing other important components such as reactant solubility limits, mass transport limitations and the design of the reactor.

Further development lies in understanding the charge transfer processes in widely utilized heterojunction schemes, specifically the perovskite–electrolyte interface. To further expand the scope of halide perovskite based photocatalytic systems, utilization of other forms of CO_2 and targeting alternative oxidation reactions is indispensable.

Author contributions

S. Shukla: conceptualization and writing – original draft. V. Jose and S. Shukla: reviewing and editing. N. Mathews: conceptualization, supervision, reviewing and editing.

Data availability

No primary research results, software or code have been included and no new data were generated or analysed as part of this review.

Conflicts of interest

There are no conflicts to declare.

Acknowledgements

S. S. acknowledges funding from the European Union's Horizon Europe program under the Marie Skłodowska-Curie Grant Agreement No. 101067667. S. S. and V. J. acknowledge Catalisti VLAIO (Vlaanderen Agentschap Innoveren & Ondernemen) for their funding through the Moonshot SYN-CAT project (HBC.2020.2614), and the Belgian federal government through the Energy Transition Fund for T-REX project. NM would like to acknowledge the funding from the National Research Foundation (NRF), Singapore, under its Competitive Research Program (CRP) (NRF-CRP25-2020-0002). The authors would like to thank Dr Tom Aernouts and Prof. Bart Vermang for fruitful discussions.

References

1 S. Chu and A. Majumdar, *Nature*, 2012, **488**, 294–303.
2 B. Obama, *Science*, 2017, **355**, 126–129.
3 M. Victoria, N. Haegel, I. M. Peters, R. Sinton, A. Jäger-Waldau, C. del Cañizo, C. Breyer, M. Stocks, A. Blakers, I. Kaizuka, K. Komoto and A. Smets, *Joule*, 2021, **5**, 1041–1056.
4 P. De Luna, C. Hahn, D. Higgins, S. A. Jaffer, T. F. Jaramillo and E. H. Sargent, *Science*, 2019, **364**, eaav3506.
5 E. Papadis and G. Tsatsaronis, *Energy*, 2020, **205**, 118025.
6 N. S. Lewis and D. G. Nocera, *Proc. Natl. Acad. Sci. U. S. A.*, 2006, **103**, 15729–15735.
7 J. M. Tarascon and M. Armand, *Nature*, 2001, **414**, 359–367.
8 A. Fujishima and K. Honda, *Nature*, 1972, **238**, 37–38.
9 M. Halmann, *Nature*, 1978, **275**, 115–116.
10 H. Nishiyama, T. Yamada, M. Nakabayashi, Y. Maehara, M. Yamaguchi, Y. Kuromiya, Y. Nagatsuma, H. Tokudome, S. Akiyama, T. Watanabe, R. Narushima, S. Okunaka, N. Shibata, T. Takata, T. Hisatomi and K. Domen, *Nature*, 2021, **598**, 304–307.
11 C.-C. Yang, Y.-H. Yu, B. van der Linden, J. C. S. Wu and G. Mul, *J. Am. Chem. Soc.*, 2010, **132**, 8398–8406.
12 S. Liu, J. Li, W. Xiao, R. Chen, Z. Sun, Y. Zhang, X. Lei, S. Hu, M. Kober-Czerny, J. Wang, F. Ren, Q. Zhou, H. Raza, Y. Gao, Y. Ji, S. Li, H. Li, L. Qiu, W. Huang, Y. Zhao, B. Xu, Z. Liu, H. J. Snaith, N.-G. Park and W. Chen, *Nature*, 2024, DOI: 10.1038/s41586-024-07723-3.
13 Y.-F. Xu, M.-Z. Yang, B.-X. Chen, X.-D. Wang, H.-Y. Chen, D.-B. Kuang and C.-Y. Su, *J. Am. Chem. Soc.*, 2017, **139**, 5660–5663.

14 L. Ding, F. Bai, B. Borjigin, Y. Li, H. Li and X. Wang, *Chem. Eng. J.*, 2022, **446**, 137102.
15 G. Wang, Z. Chen, T. Wang, D. Wang and J. Mao, *Angew. Chem., Int. Ed.*, 2022, **61**, e202210789.
16 Y. Wang, X. Liu, X. Han, R. Godin, J. Chen, W. Zhou, C. Jiang, J. F. Thompson, K. B. Mustafa, S. A. Shevlin, J. R. Durrant, Z. Guo and J. Tang, *Nat. Commun.*, 2020, **11**, 2531.
17 T. Kunene, L. Xiong and J. Rosenthal, *Proc. Natl. Acad. Sci. U. S. A.*, 2019, **116**, 9693–9695.
18 M. B. Ross, P. De Luna, Y. Li, C.-T. Dinh, D. Kim, P. Yang and E. H. Sargent, *Nat. Catal.*, 2019, **2**, 648–658.
19 D. Li, K. Yang, J. Lian, J. Yan and S. Liu, *Adv. Energy Mater.*, 2022, **12**, 2201070.
20 H. Wan, A. Bagger and J. Rossmeisl, *J. Phys. Chem. Lett.*, 2022, **13**, 8928–8934.
21 C. R. Lhermitte and K. Sivula, *ACS Catal.*, 2019, **9**, 2007–2017.
22 T. Fuchigami, S. Inagi and M. Atobe, Appendix B: *Tables of Physical Data. Fundamentals and Applications of Organic Electrochemistry*, John Wiley & Sons, 2014.
23 J. Yun, Y. S. Park, H. Lee, W. Jeong, C.-S. Jeong, C. U. Lee, J. Lee, S. Moon, E. Kwon, S. Lee, S. Kim, J. Kim, S. Yu and J. Moon, *Adv. Energy Mater.*, 2024, 2401055.
24 X. Deng, R. Li, S. Wu, L. Wang, J. Hu, J. Ma, W. Jiang, N. Zhang, X. Zheng, C. Gao, L. Wang, Q. Zhang, J. Zhu and Y. Xiong, *J. Am. Chem. Soc.*, 2019, **141**, 10924–10929.
25 U. Kang, S. K. Choi, D. J. Ham, S. M. Ji, W. Choi, D. S. Han, A. Abdel-Wahab and H. Park, *Energy Environ. Sci.*, 2015, **8**, 2638–2643.
26 T. Arai, S. Sato, T. Kajino and T. Morikawa, *Energy Environ. Sci.*, 2013, **6**, 1274–1282.
27 S. Y. Lee, S. Y. Lim, D. Seo, J.-Y. Lee and T. D. Chung, *Adv. Energy Mater.*, 2016, **6**, 1502207.
28 K. Sekizawa, S. Sato, T. Arai and T. Morikawa, *ACS Catal.*, 2018, **8**, 1405–1416.
29 V. Andrei, B. Reuillard and E. Reisner, *Nat. Mater.*, 2020, **19**, 189–194.
30 C. Li, T. Wang, B. Liu, M. Chen, A. Li, G. Zhang, M. Du, H. Wang, S. F. Liu and J. Gong, *Energy Environ. Sci.*, 2019, **12**, 923–928.
31 X. Zhou, R. Liu, K. Sun, Y. Chen, E. Verlage, S. A. Francis, N. S. Lewis and C. Xiang, *ACS Energy Lett.*, 2016, **1**, 764–770.
32 T. Arai, S. Sato and T. Morikawa, *Energy Environ. Sci.*, 2015, **8**, 1998–2002.
33 Y. Sugano, A. Ono, R. Kitagawa, J. Tamura, M. Yamagiwa, Y. Kudo, E. Tsutsumi and S. Mikoshiba, *RSC Adv.*, 2015, **5**, 54246–54252.
34 T. Sekimoto, H. Hashiba, S. Shinagawa, Y. Uetake, M. Deguchi, S. Yotsuhashi and K. Ohkawa, *J. Phys. Chem. C*, 2016, **120**, 13970–13975.
35 Gurudayal, J. W. Beeman, J. Bullock, H. Wang, J. Eichhorn, C. Towle, A. Javey, F. M. Toma, N. Mathews and J. W. Ager, *Energy Environ. Sci.*, 2019, **12**, 1068–1077.
36 N. C. Deb Nath, S. Y. Choi, H. W. Jeong, J.-J. Lee and H. Park, *Nano Energy*, 2016, **25**, 51–59.
37 Y. J. Jang, I. Jeong, J. Lee, J. Lee, M. J. Ko and J. S. Lee, *ACS Nano*, 2016, **10**, 6980–6987.
38 H. S. Jeon, J. H. Koh, S. J. Park, M. S. Jee, D.-H. Ko, Y. J. Hwang and B. K. Min, *J. Mater. Chem. A*, 2015, **3**, 5835–5842.
39 Q. Jia, S. Tanabe and I. Waki, *Chem. Lett.*, 2018, 436–439.
40 T. Arai, S. Sato, K. Sekizawa, T. M. Suzuki and T. Morikawa, *Chem. Commun.*, 2019, **55**, 237–240.
41 T. N. Huan, D. A. Dalla Corte, S. Lamaison, D. Karapinar, L. Lutz, N. Menguy, M. Foldyna, S.-H. Turren-Cruz, A. Hagfeldt, F. Bella, M. Fontecave and V. Mougel, *Proc. Natl. Acad. Sci. U. S. A.*, 2019, **116**, 9735–9740.
42 M. A. Ghausi, J. Xie, Q. Li, X. Wang, R. Yang, M. Wu, Y. Wang and L. Dai, *Angew. Chem., Int. Ed.*, 2018, **57**, 13135–13139.
43 M. Schreier, F. Héroguel, L. Steier, S. Ahmad, J. S. Luterbacher, M. T. Mayer, J. Luo and M. Grätzel, *Nat. Energy*, 2017, **2**, 17087.
44 Gurudayal, J. Bullock, D. F. Srankó, C. M. Towle, Y. Lum, M. Hettick, M. C. Scott, A. Javey and J. Ager, *Energy Environ. Sci.*, 2017, **10**, 2222–2230.
45 F. Urbain, P. Tang, N. M. Carretero, T. Andreu, L. G. Gerling, C. Voz, J. Arbiol and J. R. Morante, *Energy Environ. Sci.*, 2017, **10**, 2256–2266.
46 G. M. Sriramagiri, N. Ahmed, W. Luc, K. D. Dobson, S. S. Hegedus and F. Jiao, *ACS Sustainable Chem. Eng.*, 2017, **5**, 10959–10966.
47 M. Asadi, K. Kim, C. Liu, A. V. Addepalli, P. Abbasi, P. Yasaei, P. Phillips, A. Behranginia, J. M. Cerrato, R. Haasch, P. Zapol, B. Kumar, R. F. Klie, J. Abiade, L. A. Curtiss and A. Salehi-Khojin, *Science*, 2016, **353**, 467–470.
48 M. Schreier, L. Curvat, F. Giordano, L. Steier, A. Abate, S. M. Zakeeruddin, J. Luo, M. T. Mayer and M. Grätzel, *Nat. Commun.*, 2015, **6**, 7326.
49 B. Kim, H. Seong, J. T. Song, K. Kwak, H. Song, Y. C. Tan, G. Park, D. Lee and J. Oh, *ACS Energy Lett.*, 2020, **5**, 749–757.
50 L. Q. Zhou, C. Ling, H. Zhou, X. Wang, J. Liao, G. K. Reddy, L. Deng, T. C. Peck, R. Zhang, M. S. Whittingham, C. Wang, C.-W. Chu, Y. Yao and H. Jia, *Nat. Commun.*, 2019, **10**, 4081.
51 S. Y. Chae, S. Y. Lee, S. G. Han, H. Kim, J. Ko, S. Park, O.-S. Joo, D. Kim, Y. Kang, U. Lee, Y. J. Hwang and B. K. Min, *Sustainable Energy Fuels*, 2020, **4**, 199–212.
52 W. Deng, L. Zhang, H. Dong, X. Chang, T. Wang and J. Gong, *Chem. Sci.*, 2018, **9**, 6599–6604.
53 G. Piao, S. H. Yoon, D. S. Han and H. Park, *ChemSusChem*, 2020, **13**, 698–706.
54 Z. Chen, T. Wang, B. Liu, D. Cheng, C. Hu, G. Zhang, W. Zhu, H. Wang, Z.-J. Zhao and J. Gong, *J. Am. Chem. Soc.*, 2020, **142**, 6878–6883.
55 D. Ren, N. W. X. Loo, L. Gong and B. S. Yeo, *ACS Sustainable Chem. Eng.*, 2017, **5**, 9191–9199.
56 J. H. Montoya, L. C. Seitz, P. Chakthranont, A. Vojvodic, T. F. Jaramillo and J. K. Nørskov, *Nat. Mater.*, 2017, **16**, 70–81.

57 C. Moon and B. Shin, *Discovery Mater.*, 2022, **2**, 5.
58 J. W. Yang, Y. J. Ahn, D. K. Cho, J. Y. Kim and H. W. Jang, *Inorg. Chem. Front.*, 2023, **10**, 3781–3807.
59 J. Hwang, R. R. Rao, L. Giordano, Y. Katayama, Y. Yu and Y. Shao-Horn, *Science*, 2017, **358**, 751–756.
60 S. Chen, T. Takata and K. Domen, *Nat. Rev. Mater.*, 2017, **2**, 17050.
61 K. Sivula and R. van de Krol, *Nat. Rev. Mater.*, 2016, **1**, 15010.
62 E. Pastor, M. Sachs, S. Selim, J. R. Durrant, A. A. Bakulin and A. Walsh, *Nat. Rev. Mater.*, 2022, **7**, 503–521.
63 H. Li, X. Jia, Q. Zhang and X. Wang, *Chem*, 2018, **4**, 1510–1537.
64 A. Iwase, S. Yoshino, T. Takayama, Y. H. Ng, R. Amal and A. Kudo, *J. Am. Chem. Soc.*, 2016, **138**, 10260–10264.
65 G. Giuffredi, T. Asset, Y. Liu, P. Atanassov and F. Di Fonzo, *ACS Mater. Au*, 2021, **1**, 6–36.
66 X. Li, Y. Sun, J. Xu, Y. Shao, J. Wu, X. Xu, Y. Pan, H. Ju, J. Zhu and Y. Xie, *Nat. Energy*, 2019, **4**, 690–699.
67 Y. Liu, M. Xia, D. Ren, S. Nussbaum, J.-H. Yum, M. Grätzel, N. Guijarro and K. Sivula, *ACS Energy Lett.*, 2023, **8**, 1645–1651.
68 J. Y. Kim, J.-W. Lee, H. S. Jung, H. Shin and N.-G. Park, *Chem. Rev.*, 2020, **120**, 7867–7918.
69 M. Ahmadi, T. Wu and B. Hu, *Adv. Mater.*, 2017, **29**, 1605242.
70 X. Y. Chin, A. Perumal, A. Bruno, N. Yantara, S. A. Veldhuis, L. Martínez-Sarti, B. Chandran, V. Chirvony, A. S.-Z. Lo, J. So, C. Soci, M. Grätzel, H. J. Bolink, N. Mathews and S. G. Mhaisalkar, *Energy Environ. Sci.*, 2018, **11**, 1770–1778.
71 Q. Zhang, Q. Shang, R. Su, T. T. H. Do and Q. Xiong, *Nano Lett.*, 2021, **21**, 1903–1914.
72 R. A. John, N. Yantara, S. E. Ng, M. I. B. Patdillah, M. R. Kulkarni, N. F. Jamaludin, J. Basu, Ankit, S. G. Mhaisalkar, A. Basu and N. Mathews, *Adv. Mater.*, 2021, **33**, 2007851.
73 F. Temerov, Y. Baghdadi, E. Rattner and S. Eslava, *ACS Appl. Energy Mater.*, 2022, **5**, 14605–14637.
74 E. Ugur, M. Ledinský, T. G. Allen, J. Holovský, A. Vlk and S. De Wolf, *J. Phys. Chem. Lett.*, 2022, **13**, 7702–7711.
75 H. Lin, C. Zhou, Y. Tian, T. Siegrist and B. Ma, *ACS Energy Lett.*, 2018, **3**, 54–62.
76 T. M. Koh, K. Thirumal, H. S. Soo and N. Mathews, *ChemSusChem*, 2016, **9**, 2541–2558.
77 Z. Li, M. Yang, J.-S. Park, S.-H. Wei, J. J. Berry and K. Zhu, *Chem. Mater.*, 2016, **28**, 284–292.
78 D. Niesner, M. Wilhelm, I. Levchuk, A. Osvet, S. Shrestha, M. Batentschuk, C. Brabec and T. Fauster, *Phys. Rev. Lett.*, 2016, **117**, 126401.
79 T. Etienne, E. Mosconi and F. De Angelis, *J. Phys. Chem. Lett.*, 2016, **7**, 1638–1645.
80 E. M. Hutter, M. C. Gélvez-Rueda, A. Osherov, V. Bulović, F. C. Grozema, S. D. Stranks and T. J. Savenije, *Nat. Mater.*, 2017, **16**, 115–120.
81 D. R. MacFarlane, P. V. Cherepanov, J. Choi, B. H. R. Suryanto, R. Y. Hodgetts, J. M. Bakker, F. M. Ferrero Vallana and A. N. Simonov, *Joule*, 2020, **4**, 1186–1205.
82 H. Huang, B. Pradhan, J. Hofkens, M. B. J. Roeffaers and J. A. Steele, *ACS Energy Lett.*, 2020, **5**, 1107–1123.
83 J. Wang, Y. Shi, Y. Wang and Z. Li, *ACS Energy Lett.*, 2022, **7**, 2043–2059.
84 P. Calado, A. M. Telford, D. Bryant, X. Li, J. Nelson, B. C. O'Regan and P. R. F. Barnes, *Nat. Commun.*, 2016, **7**, 13831.
85 K. Takanabe, *ACS Catal.*, 2017, **7**, 8006–8022.
86 H. Hempel, T. J. Savenjie, M. Stolterfoht, J. Neu, M. Failla, V. C. Paingad, P. Kužel, E. J. Heilweil, J. A. Spies, M. Schleuning, J. Zhao, D. Friedrich, K. Schwarzburg, L. D. A. Siebbeles, P. Dörflinger, V. Dyakonov, R. Katoh, M. J. Hong, J. G. Labram, M. Monti, E. Butler-Caddle, J. Lloyd-Hughes, M. M. Taheri, J. B. Baxter, T. J. Magnanelli, S. Luo, J. M. Cardon, S. Ardo and T. Unold, *Adv. Energy Mater.*, 2022, **12**, 2102776.
87 L. M. Herz, *ACS Energy Lett.*, 2017, **2**, 1539–1548.
88 L. Krückemeier, Z. Liu, T. Kirchartz and U. Rau, *Adv. Mater.*, 2023, **35**, 2300872.
89 Y. Chen, H. T. Yi, X. Wu, R. Haroldson, Y. N. Gartstein, Y. I. Rodionov, K. S. Tikhonov, A. Zakhidov, X. Y. Zhu and V. Podzorov, *Nat. Commun.*, 2016, **7**, 12253.
90 R. Brenes, D. Guo, A. Osherov, N. K. Noel, C. Eames, E. M. Hutter, S. K. Pathak, F. Niroui, R. H. Friend, M. S. Islam, H. J. Snaith, V. Bulović, T. J. Savenije and S. D. Stranks, *Joule*, 2017, **1**, 155–167.
91 M. Abdi-Jalebi, Z. Andaji-Garmaroudi, S. Cacovich, C. Stavrakas, B. Philippe, J. M. Richter, M. Alsari, E. P. Booker, E. M. Hutter, A. J. Pearson, S. Lilliu, T. J. Savenije, H. Rensmo, G. Divitini, C. Ducati, R. H. Friend and S. D. Stranks, *Nature*, 2018, **555**, 497–501.
92 Z. Chen, Y. Hu, J. Wang, Q. Shen, Y. Zhang, C. Ding, Y. Bai, G. Jiang, Z. Li and N. Gaponik, *Chem. Mater.*, 2020, **32**, 1517–1525.
93 X.-D. Wang, Y.-H. Huang, J.-F. Liao, Y. Jiang, L. Zhou, X.-Y. Zhang, H.-Y. Chen and D.-B. Kuang, *J. Am. Chem. Soc.*, 2019, **141**, 13434–13441.
94 F. Xu, K. Meng, B. Cheng, S. Wang, J. Xu and J. Yu, *Nat. Commun.*, 2020, **11**, 4613.
95 Y. Jiang, J.-F. Liao, H.-Y. Chen, H.-H. Zhang, J.-Y. Li, X.-D. Wang and D.-B. Kuang, *Chem*, 2020, **6**, 766–780.
96 Z.-C. Kong, J.-F. Liao, Y.-J. Dong, Y.-F. Xu, H.-Y. Chen, D.-B. Kuang and C.-Y. Su, *ACS Energy Lett.*, 2018, **3**, 2656–2662.
97 L.-Y. Wu, Y.-F. Mu, X.-X. Guo, W. Zhang, Z.-M. Zhang, M. Zhang and T.-B. Lu, *Angew. Chem., Int. Ed.*, 2019, **58**, 9491–9495.
98 Q.-M. Sun, J.-J. Xu, F.-F. Tao, W. Ye, C. Zhou, J.-H. He and J.-M. Lu, *Angew. Chem., Int. Ed.*, 2022, **61**, e202200872.
99 J. Sheng, Y. He, M. Huang, C. Yuan, S. Wang and F. Dong, *ACS Catal.*, 2022, **12**, 2915–2926.
100 Y.-F. Mu, W. Zhang, G.-X. Dong, K. Su, M. Zhang and T.-B. Lu, *Small*, 2020, **16**, 2002140.
101 J. Sheng, Y. He, J. Li, C. Yuan, H. Huang, S. Wang, Y. Sun, Z. Wang and F. Dong, *ACS Nano*, 2020, **14**, 13103–13114.
102 Z. Liu, L. Krückemeier, B. Krogmeier, B. Klingebiel, J. A. Márquez, S. Levcenko, S. Öz, S. Mathur, U. Rau, T. Unold and T. Kirchartz, *ACS Energy Lett.*, 2019, **4**, 110–117.

103 M. Stolterfoht, C. M. Wolff, J. A. Márquez, S. Zhang, C. J. Hages, D. Rothhardt, S. Albrecht, P. L. Burn, P. Meredith, T. Unold and D. Neher, *Nat. Energy*, 2018, **3**, 847–854.
104 D. W. deQuilettes, S. Koch, S. Burke, R. K. Paranji, A. J. Shropshire, M. E. Ziffer and D. S. Ginger, *ACS Energy Lett.*, 2016, **1**, 438–444.
105 I. L. Braly, D. W. deQuilettes, L. M. Pazos-Outón, S. Burke, M. E. Ziffer, D. S. Ginger and H. W. Hillhouse, *Nat. Photonics*, 2018, **12**, 355–361.
106 A. Al-Ashouri, A. Magomedov, M. Roß, M. Jošt, M. Talaikis, G. Chistiakova, T. Bertram, J. A. Márquez, E. Köhnen, E. Kasparavičius, S. Levcenco, L. Gil-Escrig, C. J. Hages, R. Schlatmann, B. Rech, T. Malinauskas, T. Unold, C. A. Kaufmann, L. Korte, G. Niaura, V. Getautis and S. Albrecht, *Energy Environ. Sci.*, 2019, **12**, 3356–3369.
107 M. Abdi-Jalebi, M. Ibrahim Dar, S. P. Senanayak, A. Sadhanala, Z. Andaji-Garmaroudi, L. M. Pazos-Outón, J. M. Richter, A. J. Pearson, H. Sirringhaus, M. Grätzel and R. H. Friend, *Sci. Adv.*, 2019, **5**, eaav2012.
108 M. Abdi-Jalebi, M. Pazoki, B. Philippe, M. I. Dar, M. Alsari, A. Sadhanala, G. Divitini, R. Imani, S. Lilliu, J. Kullgren, H. Rensmo, M. Grätzel and R. H. Friend, *ACS Nano*, 2018, **12**, 7301–7311.
109 S. S. Bhosale, A. K. Kharade, E. Jokar, A. Fathi, S.-m Chang and E. W.-G. Diau, *J. Am. Chem. Soc.*, 2019, **141**, 20434–20442.
110 A. H. Slavney, T. Hu, A. M. Lindenberg and H. I. Karunadasa, *J. Am. Chem. Soc.*, 2016, **138**, 2138–2141.
111 L. Zhou, Y.-F. Xu, B.-X. Chen, D.-B. Kuang and C.-Y. Su, *Small*, 2018, **14**, 1703762.
112 H. Huang, H. Yuan, J. Zhao, G. Solís-Fernández, C. Zhou, J. W. Seo, J. Hendrix, E. Debroye, J. A. Steele, J. Hofkens, J. Long and M. B. J. Roeffaers, *ACS Energy Lett.*, 2019, **4**, 203–208.
113 H. Wang, X. Wang, R. Chen, H. Zhang, X. Wang, J. Wang, J. Zhang, L. Mu, K. Wu, F. Fan, X. Zong and C. Li, *ACS Energy Lett.*, 2019, **4**, 40–47.
114 J. Chakkamalayath, G. V. Hartland and P. V. Kamat, *J. Phys. Chem. C*, 2021, **125**, 17881–17889.
115 T. Kirchartz, J. A. Márquez, M. Stolterfoht and T. Unold, *Adv. Energy Mater.*, 2020, **10**, 1904134.
116 O. Stroyuk, O. Raievska, J. Hauch and C. J. Brabec, *Angew. Chem., Int. Ed.*, 2023, **62**, e202212668.
117 M. Li, S. Bhaumik, T. W. Goh, M. S. Kumar, N. Yantara, M. Grätzel, S. Mhaisalkar, N. Mathews and T. C. Sum, *Nat. Commun.*, 2017, **8**, 14350.
118 J. Shamsi, A. S. Urban, M. Imran, L. De Trizio and L. Manna, *Chem. Rev.*, 2019, **119**, 3296–3348.
119 D. W. de Quilettes, S. M. Vorpahl, S. D. Stranks, H. Nagaoka, G. E. Eperon, M. E. Ziffer, H. J. Snaith and D. S. Ginger, *Science*, 2015, **348**, 683–686.
120 G. Han, T. M. Koh, J. Li, B. Febriansyah, Y. Fang, N. F. Jamaludin, Y. F. Ng, P. J. S. Rana, S. Mhaisalkar and N. Mathews, *ACS Appl. Energy Mater.*, 2021, **4**, 2716–2723.
121 G. H. Ahmed, J. K. El-Demellawi, J. Yin, J. Pan, D. B. Velusamy, M. N. Hedhili, E. Alarousu, O. M. Bakr, H. N. Alshareef and O. F. Mohammed, *ACS Energy Lett.*, 2018, **3**, 2301–2307.
122 P. J. S. Rana, B. Febriansyah, T. M. Koh, A. Kanwat, J. Xia, T. Salim, T. J. N. Hooper, M. Kovalev, D. Giovanni, Y. C. Aw, B. Chaudhary, Y. Cai, G. Xing, T. C. Sum, J. W. Ager, S. G. Mhaisalkar and N. Mathews, *Adv. Mater.*, 2023, **35**, 2210176.
123 G. Grancini and M. K. Nazeeruddin, *Nat. Rev. Mater.*, 2019, **4**, 4–22.
124 P. P. Boix, S. Agarwala, T. M. Koh, N. Mathews and S. G. Mhaisalkar, *J. Phys. Chem. Lett.*, 2015, **6**, 898–907.
125 T. M. Koh, V. Shanmugam, X. Guo, S. S. Lim, O. Filonik, E. M. Herzig, P. Müller-Buschbaum, V. Swamy, S. T. Chien, S. G. Mhaisalkar and N. Mathews, *J. Mater. Chem. A*, 2018, **6**, 2122–2128.
126 J. W. Yang, S. G. Ji, C.-S. Jeong, J. Kim, H. R. Kwon, T. H. Lee, S. A. Lee, W. S. Cheon, S. Lee, H. Lee, M. S. Kwon, J. Moon, J. Y. Kim and H. W. Jang, *Energy Environ. Sci.*, 2024, **17**, 2541–2553.
127 J. W. Yang, H. R. Kwon, S. G. Ji, J. Kim, S. A. Lee, T. H. Lee, S. Choi, W. S. Cheon, Y. Kim, J. Park, J. Y. Kim and H. W. Jang, *Adv. Funct. Mater.*, 2024, 2400806.
128 H. R. Kwon, J. W. Yang, S. Choi, W. S. Cheon, I. H. Im, Y. Kim, J. Park, G.-H. Lee and H. W. Jang, *Adv. Energy Mater.*, 2024, **14**, 2303342.
129 S. Akel, A. Kulkarni, U. Rau and T. Kirchartz, *Phys. Rev. X*, 2023, **2**, 013004.
130 Y.-F. Mu, C. Zhang, M.-R. Zhang, W. Zhang, M. Zhang and T.-B. Lu, *ACS Appl. Mater. Interfaces*, 2021, **13**, 22314–22322.
131 M. Ou, W. Tu, S. Yin, W. Xing, S. Wu, H. Wang, S. Wan, Q. Zhong and R. Xu, *Angew. Chem., Int. Ed.*, 2018, **57**, 13570–13574.
132 X.-X. Guo, S.-F. Tang, Y.-F. Mu, L.-Y. Wu, G.-X. Dong and M. Zhang, *RSC Adv.*, 2019, **9**, 34342–34348.
133 A. Pan, X. Ma, S. Huang, Y. Wu, M. Jia, Y. Shi, Y. Liu, P. Wangyang, L. He and Y. Liu, *J. Phys. Chem. Lett.*, 2019, **10**, 6590–6597.
134 E. Rathore, K. Maji, D. Rao, B. Saha and K. Biswas, *J. Phys. Chem. Lett.*, 2020, **11**, 8002–8007.
135 J. Wang, J. Wang, N. Li, X. Du, J. Ma, C. He and Z. Li, *ACS Appl. Mater. Interfaces*, 2020, **12**, 31477–31485.
136 H. Huang, J. Zhao, Y. Du, C. Zhou, M. Zhang, Z. Wang, Y. Weng, J. Long, J. Hofkens, J. A. Steele and M. B. J. Roeffaers, *ACS Nano*, 2020, **14**, 16689–16697.
137 A. Kipkorir, J. DuBose, J. Cho and P. V. Kamat, *Chem. Sci.*, 2021, **12**, 14815–14825.
138 N. Li, X. Chen, J. Wang, X. Liang, L. Ma, X. Jing, D.-L. Chen and Z. Li, *ACS Nano*, 2022, **16**, 3332–3340.
139 L. Romani, A. Speltini, C. N. Dibenedetto, A. Listorti, F. Ambrosio, E. Mosconi, A. Simbula, M. Saba, A. Profumo, P. Quadrelli, F. De Angelis and L. Malavasi, *Adv. Funct. Mater.*, 2021, **31**, 2104428.
140 Q. Zhong, M. Cao, H. Hu, D. Yang, M. Chen, P. Li, L. Wu and Q. Zhang, *ACS Nano*, 2018, **12**, 8579–8587.
141 K. Ma, X.-Y. Du, Y.-W. Zhang and S. Chen, *J. Mater. Chem. C*, 2017, **5**, 9398–9404.

142 A. F. Gualdrón-Reyes, C. A. Mesa, S. Giménez and I. Mora-Seró, *Sol. RRL*, 2022, **6**, 2200012.
143 J. Hou, S. Cao, Y. Wu, Z. Gao, F. Liang, Y. Sun, Z. Lin and L. Sun, *Chem. – Eur. J.*, 2017, **23**, 9481–9485.
144 Y. Jiang, H.-Y. Chen, J.-Y. Li, J.-F. Liao, H.-H. Zhang, X.-D. Wang and D.-B. Kuang, *Adv. Funct. Mater.*, 2020, **30**, 2004293.
145 J. T. DuBose and P. V. Kamat, *ACS Energy Lett.*, 2022, **7**, 1994–2011.
146 X. Zhu, Y. Lin, J. San Martin, Y. Sun, D. Zhu and Y. Yan, *Nat. Commun.*, 2019, **10**, 2843.
147 S. Sun, D. Yuan, Y. Xu, A. Wang and Z. Deng, *ACS Nano*, 2016, **10**, 3648–3657.
148 M. Li, S. Xu, L. Wu, H. Tang, B. Zhou, J. Xu, Q. Yang, T. Zhou, Y. Qiu, G. Chen, G. I. N. Waterhouse and K. Yan, *ACS Energy Lett.*, 2022, **7**, 3370–3377.
149 T. Takata, J. Jiang, Y. Sakata, M. Nakabayashi, N. Shibata, V. Nandal, K. Seki, T. Hisatomi and K. Domen, *Nature*, 2020, **581**, 411–414.
150 R. Das, A. Patra, S. K. Dutta, S. Shyamal and N. Pradhan, *J. Am. Chem. Soc.*, 2022, **144**, 18629–18641.
151 C. Ma, F. T. Eickemeyer, S.-H. Lee, D.-H. Kang, S. J. Kwon, M. Grätzel and N.-G. Park, *Science*, 2023, **379**, 173–178.
152 Z.-Y. Chen, N.-Y. Huang and Q. Xu, *Coord. Chem. Rev.*, 2023, **481**, 215031.
153 Y.-F. Xu, M.-Z. Yang, H.-Y. Chen, J.-F. Liao, X.-D. Wang and D.-B. Kuang, *ACS Appl. Energy Mater.*, 2018, **1**, 5083–5089.
154 A. Li, T. Wang, C. Li, Z. Huang, Z. Luo and J. Gong, *Angew. Chem., Int. Ed.*, 2019, **58**, 3804–3808.
155 L. Wang, M. Ghoussoub, H. Wang, Y. Shao, W. Sun, A. A. Tountas, T. E. Wood, H. Li, J. Y. Y. Loh, Y. Dong, M. Xia, Y. Li, S. Wang, J. Jia, C. Qiu, C. Qian, N. P. Kherani, L. He, X. Zhang and G. A. Ozin, *Joule*, 2018, **2**, 1369–1381.
156 W. Zhao, M. Ding, P. Yang, Q. Wang, K. Zhang, X. Zhan, Y. Yu, Q. Luo, S. Gao, J. Yang and Y. Xie, *EES Catal.*, 2023, **1**, 36–44.
157 S. Gao, B. Gu, X. Jiao, Y. Sun, X. Zu, F. Yang, W. Zhu, C. Wang, Z. Feng, B. Ye and Y. Xie, *J. Am. Chem. Soc.*, 2017, **139**, 3438–3445.
158 Y. A. Wu, I. McNulty, C. Liu, K. C. Lau, Q. Liu, A. P. Paulikas, C.-J. Sun, Z. Cai, J. R. Guest, Y. Ren, V. Stamenkovic, L. A. Curtiss, Y. Liu and T. Rajh, *Nat. Energy*, 2019, **4**, 957–968.
159 L. Wang, J. Wan, Y. Zhao, N. Yang and D. Wang, *J. Am. Chem. Soc.*, 2019, **141**, 2238–2241.
160 L. Hao, L. Kang, H. Huang, L. Ye, K. Han, S. Yang, H. Yu, M. Batmunkh, Y. Zhang and T. Ma, *Adv. Mater.*, 2019, **31**, 1900546.
161 P. Xia, M. Antonietti, B. Zhu, T. Heil, J. Yu and S. Cao, *Adv. Funct. Mater.*, 2019, **29**, 1900093.
162 S. Sorcar, Y. Hwang, J. Lee, H. Kim, K. M. Grimes, C. A. Grimes, J.-W. Jung, C.-H. Cho, T. Majima, M. R. Hoffmann and S.-I. In, *Energy Environ. Sci.*, 2019, **12**, 2685–2696.
163 S. Sorcar, J. Thompson, Y. Hwang, Y. H. Park, T. Majima, C. A. Grimes, J. R. Durrant and S.-I. In, *Energy Environ. Sci.*, 2018, **11**, 3183–3193.
164 Z. Jiang, W. Wan, H. Li, S. Yuan, H. Zhao and P. K. Wong, *Adv. Mater.*, 2018, **30**, 1706108.
165 T. Di, B. Zhu, B. Cheng, J. Yu and J. Xu, *J. Catal.*, 2017, **352**, 532–541.
166 G. Yin, M. Nishikawa, Y. Nosaka, N. Srinivasan, D. Atarashi, E. Sakai and M. Miyauchi, *ACS Nano*, 2015, **9**, 2111–2119.
167 H. Zhu, S. Teale, M. N. Lintangpradipto, S. Mahesh, B. Chen, M. D. McGehee, E. H. Sargent and O. M. Bakr, *Nat. Rev. Mater.*, 2023, **8**, 569–586.
168 S. Shukla, T. M. Koh, R. Patidar, J. H. Lew, P. Kajal, S. G. Mhaisalkar and N. Mathews, *J. Phys. Chem. C*, 2021, **125**, 6585–6592.
169 A. Bashir, S. Shukla, J. H. Lew, S. Shukla, A. Bruno, D. Gupta, T. Baikie, R. Patidar, Z. Akhter, A. Priyadarshi, N. Mathews and S. G. Mhaisalkar, *Nanoscale*, 2018, **10**, 2341–2350.
170 S. Park, W. J. Chang, C. W. Lee, S. Park, H.-Y. Ahn and K. T. Nam, *Nat. Energy*, 2016, **2**, 16185.
171 J. Liang, X. Han, Y. Qiu, Q. Fang, B. Zhang, W. Wang, J. Zhang, P. M. Ajayan and J. Lou, *ACS Nano*, 2020, **14**, 5426–5434.
172 A. M. K. Fehr, A. Agrawal, F. Mandani, C. L. Conrad, Q. Jiang, S. Y. Park, O. Alley, B. Li, S. Sidhik, I. Metcalf, C. Botello, J. L. Young, J. Even, J. C. Blancon, T. G. Deutsch, K. Zhu, S. Albrecht, F. M. Toma, M. Wong and A. D. Mohite, *Nat. Commun.*, 2023, **14**, 3797.
173 M. Rahaman, V. Andrei, D. Wright, E. Lam, C. Pornrungroj, S. Bhattacharjee, C. M. Pichler, H. F. Greer, J. J. Baumberg and E. Reisner, *Nat. Energy*, 2023, **8**, 629–638.
174 V. Andrei, G. M. Ucoski, C. Pornrungroj, C. Uswachoke, Q. Wang, D. S. Achilleos, H. Kasap, K. P. Sokol, R. A. Jagt, H. Lu, T. Lawson, A. Wagner, S. D. Pike, D. S. Wright, R. L. Z. Hoye, J. L. MacManus-Driscoll, H. J. Joyce, R. H. Friend and E. Reisner, *Nature*, 2022, **608**, 518–522.
175 A. Tayyebi, R. Mehrotra, M. A. Mubarok, J. Kim, M. Zafari, M. Tayebi, D. Oh, S.-h Lee, J. E. Matthews, S.-W. Lee, T. J. Shin, G. Lee, T. F. Jaramillo, S.-Y. Jang and J.-W. Jang, *Nat. Catal.*, 2024, **7**, 510–521.
176 Y. Choi, R. Mehrotra, S.-H. Lee, T. V. T. Nguyen, I. Lee, J. Kim, H.-Y. Yang, H. Oh, H. Kim, J.-W. Lee, Y. H. Kim, S.-Y. Jang, J.-W. Jang and J. Ryu, *Nat. Commun.*, 2022, **13**, 5709.
177 H. Yang, Y. Liu, Y. Ding, F. Li, L. Wang, B. Cai, F. Zhang, T. Liu, G. Boschloo, E. M. J. Johansson and L. Sun, *Nat. Commun.*, 2023, **14**, 5486.
178 I. Poli, U. Hintermair, M. Regue, S. Kumar, E. V. Sackville, J. Baker, T. M. Watson, S. Eslava and P. J. Cameron, *Nat. Commun.*, 2019, **10**, 2097.
179 Z. Zhu, M. Daboczi, M. Chen, Y. Xuan, X. Liu and S. Eslava, *Nat. Commun.*, 2024, **15**, 2791.
180 D. Hansora, J. W. Yoo, R. Mehrotra, W. J. Byun, D. Lim, Y. K. Kim, E. Noh, H. Lim, J.-W. Jang, S. I. Seok and J. S. Lee, *Nat. Energy*, 2024, **9**, 272–284.
181 L. Wang, W. Lian, B. Liu, H. Lv, Y. Zhang, X. Wu, T. Wang, J. Gong, T. Chen and H. Xu, *Adv. Mater.*, 2022, **34**, 2200723.

182 R. Fernández-Climent, A. F. Gualdrón-Reyes, M. García-Tecedor, C. A. Mesa, D. Cárdenas-Morcoso, L. Montañes, E. M. Barea, E. Mas-Marzá, B. Julián-López, I. Mora-Seró and S. Giménez, *Sol. RRL*, 2022, **6**, 2100723.
183 S.-Y. Lee, P. Serafini, S. Masi, A. F. Gualdrón-Reyes, C. A. Mesa, J. Rodríguez-Pereira, S. Giménez, H. J. Lee and I. Mora-Seró, *ACS Energy Lett.*, 2023, **8**, 4488–4495.
184 M. Saliba, *Adv. Energy Mater.*, 2019, **9**, 1803754.
185 Q. Sun, W.-J. Yin and S.-H. Wei, *J. Mater. Chem. C*, 2020, **8**, 12012–12035.
186 M. Ahmadi, M. Ziatdinov, Y. Zhou, E. A. Lass and S. V. Kalinin, *Joule*, 2021, **5**, 2797–2822.
187 S. Sun, A. Tiihonen, F. Oviedo, Z. Liu, J. Thapa, Y. Zhao, N. T. P. Hartono, A. Goyal, T. Heumueller, C. Batali, A. Encinas, J. J. Yoo, R. Li, Z. Ren, I. M. Peters, C. J. Brabec, M. G. Bawendi, V. Stevanovic, J. Fisher and T. Buonassisi, *Matter*, 2021, **4**, 1305–1322.
188 X. Li, H. Mai, J. Lu, X. Wen, T. C. Le, S. P. Russo, D. A. Winkler, D. Chen and R. A. Caruso, *Angew. Chem., Int. Ed.*, 2023, **62**, e202315002.